


12-15-2018

Optimization of Useful Hard X-ray Photochemistry

David Lewis Goldberger

David.Goldberger@Colorado.EDU

Follow this and additional works at: <https://digitalscholarship.unlv.edu/thesesdissertations>

 Part of the [Atomic, Molecular and Optical Physics Commons](#), [Engineering Science and Materials Commons](#), [Materials Science and Engineering Commons](#), and the [Physical Chemistry Commons](#)

Repository Citation

Goldberger, David Lewis, "Optimization of Useful Hard X-ray Photochemistry" (2018). *UNLV Theses, Dissertations, Professional Papers, and Capstones*. 3494.

<https://digitalscholarship.unlv.edu/thesesdissertations/3494>

This Thesis is protected by copyright and/or related rights. It has been brought to you by Digital Scholarship@UNLV with permission from the rights-holder(s). You are free to use this Thesis in any way that is permitted by the copyright and related rights legislation that applies to your use. For other uses you need to obtain permission from the rights-holder(s) directly, unless additional rights are indicated by a Creative Commons license in the record and/or on the work itself.

This Thesis has been accepted for inclusion in UNLV Theses, Dissertations, Professional Papers, and Capstones by an authorized administrator of Digital Scholarship@UNLV. For more information, please contact digitalscholarship@unlv.edu.

OPTIMIZATION OF USEFUL HARD X-RAY PHOTOCHEMISTRY

By

David L. Goldberger

Bachelor of Arts – Physics
University of Colorado at Boulder
2015

Bachelor of Fine Arts – Theatrical Performance
University of Colorado at Boulder
2015

A thesis submitted in partial fulfillment
of the requirements for the

Master of Science - Physics

Department of Physics and Astronomy
College of Sciences
The Graduate College

University of Nevada, Las Vegas
December 2018

Copyright 2018 David Goldberger

All Rights Reserved



Thesis Approval

The Graduate College
The University of Nevada, Las Vegas

October 31, 2018

This thesis prepared by

David L. Goldberger

entitled

Optimization of Useful Hard X-Ray Photochemistry

is approved in partial fulfillment of the requirements for the degree of

Master of Science - Physics
Department of Physics and Astronomy

Michael Pravica, Ph. D.
Examination Committee Chair

Kathryn Hausbeck Korgan, Ph.D.
Graduate College Interim Dean

Stephen Lepp, Ph. D.
Examination Committee Member

Eunja Kim, Ph. D.
Examination Committee Member

Paul Forster, Ph. D.
Graduate College Faculty Representative

Abstract

X-ray induced damage is generally considered a nuisance, but in the field of *Useful Hard X-ray Photochemistry* we harness the highly ionizing and penetrating properties of hard X-rays (> 7 keV) to initiate novel photochemical decomposition and synthesis at ambient and extreme conditions. Preliminary experiments suggest that the energy of irradiating photons and the sample pressure play roles in determining the nature of X-ray induced damage. Here, we present the X-ray energy dependence of damage induced in strontium oxalate, strontium nitrate, and barium nitrate, as well as the pressure dependence of X-ray induced damage of strontium oxalate. Our results indicate that the rate of X-ray induced damage and in some case the products depend on the energy of the irradiating X-rays and on the sample pressure. These results allow us to control and optimize *Useful Hard X-ray Photochemistry* so that we can mitigate unwanted X-ray damage and harness useful reactions.

Acknowledgements

I gratefully acknowledge support from the Department of Energy National Nuclear Security Administration (DOE-NNSA) under Award Number DE-NA0002912. I also acknowledge support from the DOE Cooperative Agreement No. DE-FC08-01NV14049 with the University of Nevada, Las Vegas. Portions of this work were performed at HPCAT (Sector 16), Advanced Photon Source (APS), Argonne National Laboratory. HPCAT operation is supported by DOE-NNSA under Award No. DE-NA0001974, with partial instrumentation funding by the NSF. The Advanced Photon Source is a U.S. Department of Energy (DOE) Office of Science User Facility operated for the DOE Office of Science by Argonne National Laboratory under Contract No. DE-AC02-06CH11357. This research was sponsored in part by the National Nuclear Security Administration under the Stewardship Science Academic Alliances program through DOE Cooperative Agreement #DE-NA0001982.

Additionally, I gratefully acknowledge the support and guidance of my mentor and thesis advisor, Dr. Michael Pravica. Without Dr. Pravica none of this work would have been possible.

Dedicated to my parents for fostering my natural curiosity and for all their love and support

Table of Contents

Abstract	iii
Acknowledgements	iv
List of Figures	vii
List of Equations	viii
Chapter 1 - Introduction	1
Motivation	1
Background information	3
X-ray Fundamentals and the Production of X-rays	3
X-ray Interactions with Matter	7
X-ray Diffraction and the Basics of Crystallography	8
Raman Spectroscopy	12
The Diamond Anvil Cell	12
Chapter 2 – Strontium Oxalate	15
Introduction	15
Experiment	16
Results and Analysis	18
Energy Dependence	18
Pressure Dependence	24
Summary and Conclusions	29
Chapter 3 – Barium and Strontium Nitrate	31
Introduction	31
Experiment	33
Results and Analysis	35
Visual Evidence	35
Raman Spectroscopy	35
X-ray Diffraction	37
Summary and Conclusions	44
Chapter 4 – Conclusions and Future Work	46
References	52
Curriculum Vitae	55

List of Figures

Figure 1. The Electromagnetic Spectrum.....	4
Figure 2. Example Diffraction pattern and corresponding Diffractogram.....	11
Figure 3. (a) X-ray tomography of strontium oxalate (b) Visual evidence of Modification.....	18
Figure 4. (a) Diffraction patterns of strontium oxalate (b) Unit cell of strontium oxalate.....	19
Figure 5. Kinetics of loss of strontium oxalate crystallinity at various energies.....	21
Figure 6. Final loss of crystallinity as a function of energy.....	23
Figure 7. Initial diffractograms of strontium oxalate at various pressures.....	25
Figure 8. Kinetics of loss of strontium oxalate crystallinity at various pressures.....	26
Figure 9. Final loss of crystallinity as a function of pressure.....	28
Figure 10. Unit cells of (a) barium and (b) strontium nitrate.....	32
Figure 11. Pre- and Post-Irradiation pictures of samples of barium nitrate.....	34
Figure 12. Pre- and Post-Irradiation Raman spectra of (a) barium and (b) strontium nitrate.....	36
Figure 13. Pre- and Post-Irradiation Diffractograms of (a) barium and (b) strontium nitrate.....	37
Figure 14. Loss of crystallinity as a function of fluence for (a) barium and (b) strontium nitrate.....	40
Figure 15. Change of FWHM as a function of fluence for (a) barium and (b) strontium nitrate.....	41
Figure 16. Unit cell volume change as a function of fluence for (a) barium and (b) strontium nitrate.....	43

List of Equations

Equation 1. Relation of photon energy, frequency, and wavelength	4
Equation 2. Bragg's law	9
Equation 3. Loss of crystallinity as a function of time	19
Equation 4. Loss of crystallinity in the frame of the Avrami Model	20
Equation 5. Chemical equation for the decomposition of the nitrate anion	31
Equation 6. Change of parameters as a function of fluence	38
Equation 7. Loss of crystallinity as a function of fluence	38
Equation 8. Volume change as a function of fluence	42

Chapter 1 - Introduction

Motivation

In December of 1895, the German physicist Wilhelm Röntgen submitted a paper titled, "On a New Kind of Rays" to the Würzburg's Physical-Medical journal.¹ In the paper, Röntgen explained that he observed fluorescence on a screen even after isolating a discharge tube from visible light. He concluded that a new kind of ray induced the fluorescence he observed, and he named the new rays, "X-rays". Röntgen's discovery galvanized communities of scientists and doctors to experiment with X-rays, and the world quickly realized their utility. The impact of the discovery cannot be overstated. Röntgen was awarded the inaugural Nobel Prize in physics for his work, and in the year following his paper, 49 essays and 1044 articles concerning X-rays were published.² One aspect of X-rays that became clear almost immediately, was their potential to damage or otherwise alter organic and inorganic materials through photochemical processes.

The work of professor John Daniel and Dr. William Dudley of Vanderbilt University is emblematic of the discovery of X-ray hazards. In February 1896, the researchers wanted to use new X-ray imaging technology to locate a bullet in the head of a child who had been shot and survived, but they were concerned about the safety of the child. To alleviate these concerns, Dr. Dudley volunteered to test the technology by placing an X-ray emission tube about half an inch from his skull. Twenty-one days after irradiation, Daniel reported that he noticed a two-inch bald spot growing where Dudley's head had been exposed.³ The Vanderbilt researchers were not unique in their eagerness to make use of the new technology, many other researchers faced similar and worse fates while discovering X-ray hazards. Reports of X-ray induced damage to inorganic materials were common as well, though they were less dramatic than their organic counter parts.

Since the discovery of the potential hazards of X-ray photochemistry, it has generally been considered a nuisance. Besides the health risks, the damage caused by X-ray photochemistry presented other challenges to early researchers. For example, crystallographers using X-ray diffraction to determine crystal lattice structures often blamed X-ray damage when they could not interpret their data.⁴ As X-ray and other radiative sources became more ubiquitous and more powerful, avoiding radiation damage became an important engineering problem. To this day, researchers continue to search for materials that are more resilient to radiation damage for use in nuclear, and synchrotron facilities.⁵⁻⁷ While radiation damage generally encompasses various types of radiation, the damage caused by X-rays is often of primary concern.

Recent findings in diverse fields challenge the prevailing negative view of X-ray photochemistry. For example, the search for cancer treatment processes that can selectively damage cancerous cells, motivated researchers to consider X-ray photochemistry from a different perspective. Many years of research have been devoted to using targeted X-rays for cancer treatment and they are summarized elsewhere.⁸ One recent study claims that X-ray induced bond breaking reactions have been successful in selectively destroying cancerous cells in rats.^{8,9} Cancer treatments and other uses for X-ray induced damage are stimulating, the potential for X-ray photochemistry to enable synthesis of novel compounds is arguably more exciting. For instance, it has been proposed that recently observed complex molecules in the interstellar medium may be remnants of X-ray photochemical reactions.¹⁰ One major goal in the developing field of *useful hard X-ray photochemistry* is to identify additional useful X-ray driven photochemical reactions.

Research in *useful hard X-ray photochemistry* seeks to harness and control X-ray photochemistry to employ damage when useful, and to synthesize new materials when possible. So far, X-ray driven decomposition reactions have been used to produce molecular gasses, such as Cl₂,¹¹ O₂,¹² and F₂.¹³ Additionally, novel materials, including a new type of CsO₂,¹⁵ OF₂,¹⁶ and possibly CsF₂, and CsF₃,¹⁷ have

been synthesized via X-ray induced photochemical reactions. The results of these preliminary experiments suggest that X-ray photochemistry is a useful tool, in the correct conditions. However, the full utility of X-ray photochemistry cannot be realized until the processes can be optimized for various reactions.

The successful X-ray photochemistry experiments described above were performed at synchrotron beamlines with tightly focused X-ray beams of high photon flux. As such, the experiments require large amounts of energy and only generate small amounts of reaction products. The reaction products are often interesting enough to warrant such studies despite the inefficiency of the photochemical processes, but more efficient production is desirable. Improving our understanding of the mechanisms of X-ray induced photochemistry is a crucial first step in optimizing desirable photochemical processes to increase the efficiency of useful X-ray driven reactions. This thesis summarizes early attempts to improve the efficiency of useful X-ray photochemical reactions.

The first section of this thesis provides background information intended to improve understanding of X-ray photochemistry and the analytical techniques used. In the second section, the preliminary experiment on the pressure and energy dependence of X-ray induced modifications of strontium oxalate is discussed. A second experiment on the energy dependence of X-ray induced damage of barium and strontium oxalate is presented in the third section. Finally, the experimental results and conclusions drawn from these results are summarized in the concluding section of the thesis.

Background information

X-ray Fundamentals and the Production of X-rays

An X-ray is a type of light. Light is an excitation of the electromagnetic field, which can be described as an electromagnetic (EM) wave, or as a particle called a photon. Characteristics of light, like the color of visible light, depend on the frequency or wavelength of the EM wave. EM radiation, or photons, with

shorter wavelengths have higher frequencies and higher energies because these characteristics are related by:

$$E = h f = \frac{h c}{\lambda} \quad (1)$$

Where E is the energy of the photon, f is the frequency, and λ is the wavelength. The other two values that appear in equation 1 are planks constant, $h \cong 6.626 \times 10^{-34}$ Js, and the speed of light, $c = 299,792,458 \frac{m}{s}$. Since each of the characteristics are related by equation 1, specifying one defines the others. The standard for describing a photon varies between disciplines. For this thesis, photons will be described by their energies. Different types of light are categorized according to where they fall on the EM spectrum, as shown in figure 1.¹⁸

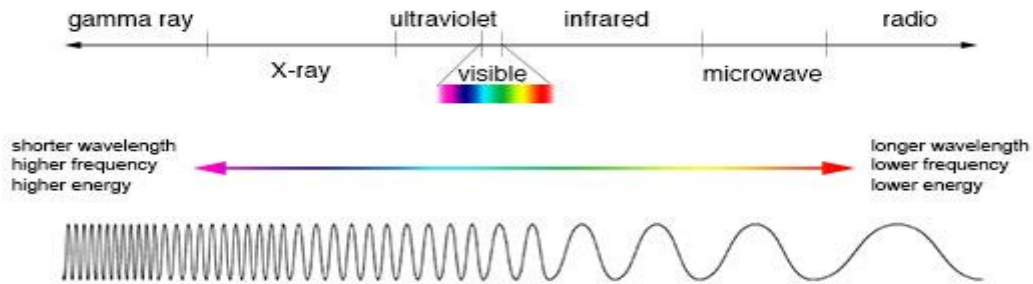


Figure 1. A schematic representation of the electromagnetic spectrum. X-rays fall between gamma rays and ultraviolet radiation. X-rays have shorter wavelength, higher frequency and higher energy than visible light. This figure has been reproduced from reference 18.

Generally, photons of energy between 100 eV and 100 keV are considered X-ray photons. Note that the energy of photons considered X-rays can vary by three orders of magnitude. An X-ray photon of 100 keV interacts with matter differently than an X-ray photon of 100 eV. As such, X-rays are often further broken down into two subcategories: soft and hard X-rays. The division between soft and hard X-rays varies somewhat, but generally X-rays of energy less than 7 keV are considered soft while those with energy greater than 7 keV are hard. The characteristics of X-rays are often determined by the means of their production.

There are many systems that can produce X-rays, but a synchrotron is the optimal source of X-rays for use in driving photochemical reactions. A synchrotron is a cyclic particle accelerator that produces X-rays via Bremsstrahlung radiation from the deceleration of relativistic electrons.¹⁹ Bremsstrahlung, or braking radiation, is produced when a charged particle is decelerated. There are three key advantages of using a synchrotron to produce X-rays. Firstly, Bremsstrahlung radiation is broadband, meaning that it will produce X-rays of various energies. To understand the energy dependence of X-ray induced photochemical processes we must be able to produce X-rays of several different energies. Secondly, synchrotrons produce significantly higher photon flux than other radiation sources. Higher photon flux increases the probability that an X-ray driven reaction will occur which makes it desirable. Finally, synchrotron sources have high brilliance. Brilliance is a measure of brightness and the angular extent of radiation. Brightness is proportional to photon flux, but two sources that have the same brightness can have different brilliance. For example, a laser and a lightbulb may have the same brightness, but the laser will have high brilliance, whereas the lightbulb will have low brilliance.^{20, 21} High brilliance, or more specifically low angular spread, is critical because a beam of low angular spread can be focused more, and a tightly focused beam is often ideal for experiments in X-ray photochemistry.

The experiments described in this thesis were performed at the 16 BM-D beamlines of a synchrotron called the advanced photon source (APS) at the Argonne National Lab in Chicago. In the APS

electrons are accelerated by a series of particle accelerators to 99.999999% of the speed of light.²² After accelerating the electrons, they are transferred to a storage ring where they are focused into a beam that circulates at a constant radius. To produce X-rays, electrons are removed from the storage ring and decelerated such that they produce Bremsstrahlung radiation. The removal and deceleration are accomplished either by bending magnets (beamlines designated BM) or insertion devices (beamlines designated ID). Insertion devices are newer technology that produce more Bremsstrahlung radiation than bending magnets.²³ Most X-ray photochemistry studies have been performed at bending magnet beamlines, including those discussed here, but future studies may take advantage of the insertion device beamlines to investigate the photon flux dependence of X-ray induced processes.

A few features of the 16 BM-D beamline at the APS make it an ideal system for studying X-ray photochemistry. Firstly, there is a monochromator installed at 16 BM-D which filters the broadband (polychromatic) Bremsstrahlung radiation to produce an X-ray beam of a single energy (monochromatic). The energy resolution of the monochromator is measured as $\frac{\Delta E}{E} < 5 \times 10^{-4}$.²⁴ This resolution means that if the monochromator is set to 20 keV it will provide X-ray photons of 20 keV \pm 10 eV. Secondly, the X-ray beam produced by 16 BM-D can be focused through a series of X-ray optics to about 4x4 μm . A tightly focused X-ray beam allows for increased photon flux density and enables more experiments, which is ideal. Lastly, the photon flux of 16 BM-D is ideal for X-ray photochemistry experiments. An insertion device beamline would provide more flux, but that would hinder studies of the kinetics of X-ray photochemistry as excessive flux accelerates photochemical process such that our analytic techniques can't measure kinetics fast enough. Luckily, we had access to the 16 BM-D beamline for both sets of experiments described in this thesis.

X-ray Interactions with Matter

Fundamentally, X-ray photochemistry is driven by interactions between X-ray photons and matter. Such interactions depend greatly on the X-ray energy and the composition of matter, and to a lesser extent on the local environment in which the interaction takes place. The interactions can be grouped into two categories: scattering and absorption. Both processes are important for the study of X-ray photochemistry. There are two types of X-ray scattering: inelastic, or Compton scattering, and elastic, or Rayleigh scattering. In Compton scattering, an X-ray photon interacts with an outer shell electron, the photon donates energy to the electron, and it scatters in a random direction. In most cases, the transferred energy is used to ionize the host atom, creating a free electron and an ion, but there are other mechanisms for spending the transferred energy.²⁵ In Rayleigh scattering, an X-ray interacts with an outer shell electron without transferring energy. Rayleigh scattering from periodic structures like crystal lattices creates diffraction patterns, which can be used to analyze the structure of solids.²⁶ The use of X-ray diffraction to identify X-ray induced photochemical changes in solids is critical for studies of X-ray photochemistry, and it is discussed further in the next section. In X-ray absorption, an X-ray photon is absorbed, and its energy ionizes the interacting atom to create a photoelectron and an ion. X-ray absorption is key to inducing photochemical reactions.

The majority of X-ray induced photochemical processes are triggered by the absorption of an X-ray photon. Generally, the probability for an atom with atomic number, Z , to absorb an X-ray photon of energy, E , is proportional to $\frac{Z^3}{E^3}$.²⁷ However, in addition to this general trend, every atom has characteristic energies at which it will preferentially absorb photons. These characteristic energies correspond to the energies needed to stimulate electronic transitions between different energy levels, or to ionization potentials, and they are commonly referred to as “edges”. For example, the K-edge matches the amount of energy needed to ionize a core electron, one with the principle quantum number $n=1$, whereas the L-

edge is the amount of energy needed to ionize an electron with principle quantum number $n=2$.²⁸ Absorption of an X-ray photon often leaves an atom in an unstable state from which it will decay by triggering complex relaxation processes.

The relaxation process of an atom that has become unstable due to ionization upon the absorption of an X-ray photon is a complex probabilistic progression through one or more possible relaxation channels. Discussion of the various possible relaxation channels is beyond the scope of this paper, but it is presented elsewhere.¹⁵ To summarize, after an electron is ionized, it leaves behind a hole that can be filled by an electron of higher energy (with a higher principle quantum number) which will make the host atom more stable. However, to fill the hole, the electron must give up some energy which must be consumed elsewhere. Excess energy is often consumed via the creation and emission of a photon. Alternatively, the host atom can consume the excess energy by ejecting an outer electron with additional kinetic energy. This is referred to as the Auger effect, and the ejected electron is called an Auger electron.⁸ Interestingly, in multiatomic bound systems like molecules or ionic solids, energy can also be consumed via an inter-atomic auger effect, which is when an auger electron is emitted from an atom that was bound to the absorbing atom.²⁹ Other possible relaxation channels include intermolecular coulomb decay, and electron transfer mediated decay which are described elsewhere.^{15, 30, 31} Depending on how the atom relaxes, absorption of an X-ray photon can induce photochemical changes that drastically alter the properties of the atom.

X-ray Diffraction and the Basics of Crystallography

One of the earliest and most powerful uses of X-rays is X-ray diffraction. Diffraction patterns are produced from the constructive interference of Rayleigh scattered X-rays from periodic structures like crystal lattices. The effect was first observed in 1913 by the father and son team of William Henry and Lawrence Bragg.³² The Braggs were surprised by the reproducible periodic patterns formed by X-rays

reflected off of crystalline solids, and by the fact that changing the angle of incidence and the energy of X-rays they could modulate the reflected intensity by creating zones of constructive interference. Upon further investigation, they proposed Bragg's law that relates the angle of incidence, θ , the wavelength of incident photons, λ , and the interplanar spacing, d as:

$$2d \sin \theta = n \lambda \quad (2)$$

where n is a positive integer. The Braggs revolutionized crystallography with this relation, as they could use it to directly measure the interplanar spacing of crystalline structures. When multiple different interplanar spacings, or diffraction planes, existed within a crystal, they could be investigated by physically rotating it relative to incident X-rays. Thus, X-ray diffraction became the quintessential tool for determining the structure of crystals.

Crystallography, the experimental study of the arrangement of atoms in crystalline solids, was well established before the advent of the X-ray, but the Bragg's discovery significantly improved measurement capabilities. Before X-ray diffraction, crystals were studied based on the geometric properties and symmetry. Despite the relatively rudimentary methods of early crystallographers, they made significant discoveries. In 1801 the French priest and pioneering crystallographer, René Just Haüy, published a book called *Traité de Minéralogie*. One of the groundbreaking ideas in his book was the concept of the unit cell, or what he called an "integrant molecule".³³ The unit cell is the fundamental building block of a crystal. It is repeated along three different principle axes to build up a crystal. Interestingly, the principle axes of a crystal are not always perpendicular. The species and arrangement of atoms in a crystal's unit cell, along with the three principle axes over which the unit cell repeats, determine the physical and chemical properties of a crystal. Following Haüy's work, William Hallows Miller developed a labeling system called Miller Indices for identifying different faces of a crystal, in 1839.³⁴ Miller indices are still used today; diffraction planes, for example, are labeled by their Miller indices. While these concepts were well established theoretically, X-ray diffraction provided the first

means to experimentally measure dimensions of unit cells with considerable accuracy. X-ray diffraction is commonly paired with high pressure techniques to investigate structural transformations, or phase changes, that many materials exhibit upon pressurization. Such structural phase changes are often accompanied by various changes of the materials' properties. Over time, X-ray diffraction techniques grew more sophisticated and more accurate. Today there are many variants of X-ray diffraction that are useful for interrogating a variety of physical systems.

Angularly dispersive powder X-ray diffraction (ADXRD) is a modification of the Bragg's original technique that allows for more efficient data collection. The fundamental physics of ADXRD is still described by Bragg's law, but the key difference is that rather than reflecting X-rays off a single crystal at a known angle, X-rays are reflected off a powder of randomly oriented micro-crystal grains and they are collected on a two-dimensional area detector. Constructive interference from various accessible interplanar spacings in the powder sample produces concentric cones, which are imaged as Debye-Scherrer rings on the detector.³⁵ Generally, diffraction patterns are presented as a diffractogram in which the intensity of reflected X-rays is plotted vs the angle at which they were detected. We depend on a program called Dioptas[®] to produce diffractograms as shown in figure 2 below.³⁶ Peaks in the diffractogram correspond to constructive interference from different planes within the sample, which can be specified according to their Miller Indices.

Diffraction patterns are sensitive to the experimental conditions in which they are measured, so analysis based on changes of diffraction patterns must be done carefully. For analysis of the experiments presented below, three aspects of diffraction peaks are particularly important: The position, breadth, and the integrated intensity of peaks. The position of diffraction peaks in a diffractogram gives information about the crystalline structure of the material. The exact position of a peak will shift if the corresponding interplanar spacing within the crystalline sample changes. Such shifts are often observed upon pressurization. The breadth of a diffraction peak can give information about the local micro-structure of

a sample, including the presence of inhomogeneous strain, and estimations of average micro-crystal grain size. However, diffraction peak breadth also depends on the resolution of the system measuring the diffraction pattern. Some systems will introduce instrumental broadening effects and the final breadth of the diffraction peak will be a convolution of the instrumental broadening and the intrinsic sample broadening. There are many factors that influence the intensity of diffraction peaks, but our experiments are designed to minimize these unwanted effects. The sample temperature, orientation of the X-ray beam relative to the sample, polarization of the X-ray beam, preferred orientation of crystals in the sample, and thickness of the sample can all modulate the intensities of diffraction peaks. In experiment we avoid these modulations by avoiding heating and keeping all other parameters constant. Doing so ensures that any changes we observe in the diffraction patterns are due to X-ray interactions, rather than one of aforementioned parameters.

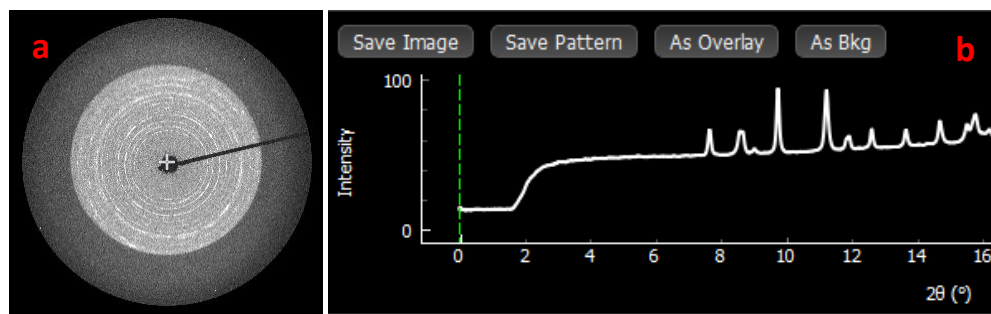


Figure 2. Shows an example of a diffraction pattern of strontium oxalate. **(a)** the Debye-Scherrer rings as they appear on the two-dimensional detector, **(b)** the diffractogram corresponding to A. Note that we always perform a background subtraction, not shown in **(b)**, before analyzing the data.

Raman Spectroscopy

Raman spectroscopy is a powerful tool for analyzing changes induced by X-ray photochemistry. Raman spectroscopy is based on the principles of Stokes and anti-stokes scattering. As mentioned above, when light interacts with an atom it can scatter elastically or inelastically. Elastic, or Rayleigh, scattering occurs if an electron in the target atom is excited to a virtual state and then returns to its initial state, emitting a photon of energy equal to the incident photon. In some cases, an excited electron can return to a state that is one vibrational level higher or lower than its initial state. When the electron returns to a higher vibrational state, it emits a photon of energy less than the incident photon, and the process is called Stokes's scattering. Anti-stokes scattering occurs when an electron returns to a lower vibrational state. To perform Raman spectroscopy a laser light is shown on a sample, the reflected light is collected, and filter is used to remove elastically scattered photons. The energy difference between the collected photons and the incident photons is called the Raman Shift and it is commonly recorded in units of cm^{-1} . Since the Raman shift corresponds to the difference in energy between vibrational levels it can be used to identify the energy of phonons in a system, which in turn can be used to discern the nature of chemical bonds in an unknown system. In this sense, Raman spectroscopy provides the structural fingerprint of a sample.³⁷ Note that infrared (IR) spectroscopy also depends on exciting transitions between vibrational states, so it gives similar information to Raman spectroscopy. Often IR spectroscopy and Raman are used to complement one another.

The Diamond Anvil Cell

The Diamond Anvil Cell (DAC) is another useful tool for performing experiments in useful hard X-ray photochemistry. In material science DACs are commonly used to provide extreme pressures. Their operation is based on the fundamental principle that pressure is equal to force divided by area. DAC design

vary widely, but a few features are common to all DACs. Firstly, diamonds used in DAC's are polished to have a minute flat surface called a culet. Culet size varies but usually it's 50-500 μm in diameter depending on the intended pressure. Secondly, the diamonds are mounted to opposing pistons with considerably larger areas. Force is applied to the pistons via hand rotated screws or by increasing gas pressure on a membrane. The squeezing force applied to opposing pistons creates extreme pressures due to the minute area of the diamond culets. Finally, a metallic gasket, usually made of stainless steel or rhenium, with a small sample chamber is used to confine the sample and stabilize the diamonds as pressure increases. DACs have been used to reach extreme pressures up to a few megabar (a few million times atmospheric pressure).^{38,39} Pressure in DACs are usually measured in gigapascals (GPa) - one GPa is equal to 10^9 N/m^2 . Besides the ability to produce extreme pressures, DACs have other advantages.

DACs were popularized because they can provide extreme pressures, but they have additional advantages that make them ideal for studies of X-ray photochemistry. Diamonds interact with light, but they are almost transparent to X-rays of energy greater than 10-12 keV. High energy X-rays pass through the diamonds in a DAC like windows. In practice, we always correct the measured flux of incident photons based on the known absorption of diamond at a given photon energy, but these corrections are small. Diamonds are also transparent to visible light, which is a great advantage because it allows for optical spectroscopy, like Raman, on samples inside of DACs. Another benefit of the DAC is the high thermal conductivity of diamonds and the mass of the diamonds relative to the sample. If the sample in the DAC makes good thermal contact with the diamonds, heat created by irradiating the sample will be thermally conducted into the diamonds and the temperature of the system will increase much less than if the sample was thermally isolated. Pressurizing a DAC creates a seal between the diamonds and the gasket material, this seal can be created at pressures as low as 0.1-0.5 GPa depending on the geometry of the DAC and the gasket material. X-ray induced decomposition reactions can produce gasses which could escape from an unsealed system, so a sealed system is ideal. Using a DAC pressurized to $< 0.5 \text{ GPa}$ provides

a sealed, thermally conductive, optically accessible environment in which X-ray photochemistry can proceed and be observed.

Without a dependable method to measure pressure, a DAC is useless. While there are a few techniques for measuring pressure, the most common is to use the shift of the ruby R_1 fluorescence line. As is common in physics, we depend on previous work that calibrated the shift of the ruby fluorescence line as a function of pressure.^{40, 41} Then by loading a ruby in the sample chamber of the DAC along with our sample, measuring its fluorescence and comparing to the calibration curve we get an accurate measure of pressure. One important limitation of this technique is that it depends to some extent on the hydrostaticity of the sample chamber. If the sample chamber is not hydrostatic, and the ruby is not adjacent to the sample, then the pressure measured by the ruby may be different than the pressure that the sample experiences. Often this issue is mitigated by adding a pressure transmitting medium, ideally a fluid which supports no shear, to equalize the pressure within the sample chamber.⁴² However, adding a PTM to the sample chamber is not good for studies of X-ray photochemistry because the PTM is another compound that could influence the photochemical processes. Instead we attempt to place rubies in the center of our sample chambers, and then we pack the sample chamber full of sample. This process creates a quasi-hydrostatic environment, and we recognize some unavoidable error in our pressure measurements due to the lack of hydrostacity in the sample chambers.

Chapter 2 – Strontium Oxalate

Introduction

In 2016, the Pravica group synthesized a new carbon monoxide derived (CO-derived) material by irradiating powdered crystalline strontium oxalate (SrC_2O_4) with high flux polychromatic X-rays.^{43, 44} The new material exhibited characteristics similar to polymeric carbon monoxide (PCO), which is of particular interest due to its high energy density. The experiment was an early example of *useful hard X-ray photochemistry*. Previously, only milligrams of PCO could be synthesized, and the process required high-pressure and laser heating. The prospect of a more efficient synthesis method for producing a highly energetic PCO-like material motivated the measurements of the energy and high-pressure dependence of X-ray induced modifications of crystalline strontium oxalate. This work serves two purposes, First, it leads to optimization of the X-ray induced synthesis of the novel, useful CO-derived material, and second it provides insight into the mechanism of X-ray photochemistry in solids which may be applicable to other X-ray photochemical processes.

Previous work suggested two parameters of the experimental synthesis of novel CO-derived material that are experimentally controllable and that may impact the efficiency of the process. One previous study showed that X-ray induced decomposition of ionic salts, like KClO_3 , depends on the irradiating photon energy.⁴⁵ Other experiments showed that the application of pressure can control the decomposition rate of X-ray photochemical reactions.^{12, 46} One study found that X-ray induced decomposition may occur differently depending on the structural phase of the material. This phenomenon was deemed *phase-dependent decomposition*.⁴⁷ Together these results prompt attempts to study the energy and high-pressure dependence of X-ray induced synthesis of CO-derived material from irradiation of crystalline strontium oxalate. Note that the work presented in this section of the thesis is also discussed

in our publication entitled *Measurement of the Energy and High-Pressure Dependence of X-ray-Induced Decomposition of Crystalline Strontium Oxalate*.⁴⁸

Experiment

To investigate the energy and high-pressure dependence of X-ray induced synthesis, we performed two sets of experiments at the 16 BM-D beamlines of the APS. The beamline characteristics, and analysis method was similar for both experiments. The 16 BM-D monochromator was used to set the energy of the irradiating X-ray beam. The beam size varied with energy but was always less than 4 x 4.2 μm FWHM horizontally and vertically respectively. The sample was placed at the focus of the X-ray beam, and ADXRD patterns were collected every minute over an hour of irradiation using a Mar345 image plate detector. An ion chamber directly upstream of the DAC recorded photon flux. Before and after irradiation, the sample was characterized via Raman spectroscopy. Due to the limited time to perform experiments and the tight focus of the X-ray beam relative to the size of the sample, we irradiated the sample at one spot for an hour, then translated the DAC and irradiated a new spot under modified experimental conditions (either different X-ray energy or sample pressure). Figure 3a gives an example of the orientation of various irradiated spots in a DAC. We checked the Raman spectrum before irradiating a new spot within the sample to ensure that region was virgin, unaltered SrC_2O_4 . Changes in the ADXRD patterns over the hour of irradiation, and comparison of the pre and post-irradiation Raman spectra provided information about the X-ray photochemical process.

The sample preparation and initial DAC loading was also similar in the two sets of experiments. To load the samples, we started by pre-indenting a 250 μm thick stainless-steel gasket to ~ 40 μm , using diamonds with ~ 300 μm diameter culets. An ~ 140 μm diameter hole was then drilled into the indented portion of the gasket via an electric discharge machine (EDM) to create the sample chamber. A ruby ball was placed in the center of the sample chamber, and then the sample of powdered crystalline SrC_2O_4 (Alfa

Aesar 95%) was packed into the sample chamber. Attempts were made to keep the ruby centered in the sample chamber, but the ruby often shifted unavoidably. No pressure-transmitting medium was used in these experiments. We recognize some error in the measurements of pressure due to the quasi-hydrostatic sample environment. After loading, the treatments of the sample diverged for the two experiments.

For the energy dependence experiment, the DAC was pressurized slightly to create a sealed environment while keeping the sample pressure close to ambient. The pressure measured from the shift of the ruby fluorescence was negligible (< 0.08 GPa). Various spots in the DAC were irradiated with X-ray beams of 15, 18, 20, 25, and 28 keV as shown in figure 3a. ADXRD patterns were collected once per minute over the hour of irradiation at each energy. Interestingly, when we attempted to investigate the post-irradiation Raman spectra, we found that the irradiated regions were highly fluorescent. We tried to investigate with 635, and 532 nm laser excitation sources, but in both cases the fluorescence from the irradiated sample overwhelmed the Raman signal from that irradiated region. While this was not ideal, as it precluded characterization of the irradiation products, it did provide evidence that the X-ray interaction modified the material. Figure 3b shows visual evidence of the laser-induced fluorescence within the irradiated regions of the sample. For the pressure dependence experiment, all the parameters were the same, but we set the X-ray beam energy at 20 keV and irradiated different regions in the sample as we increased the sample pressure. Again, pressure was measured by the shift of ruby fluorescence.

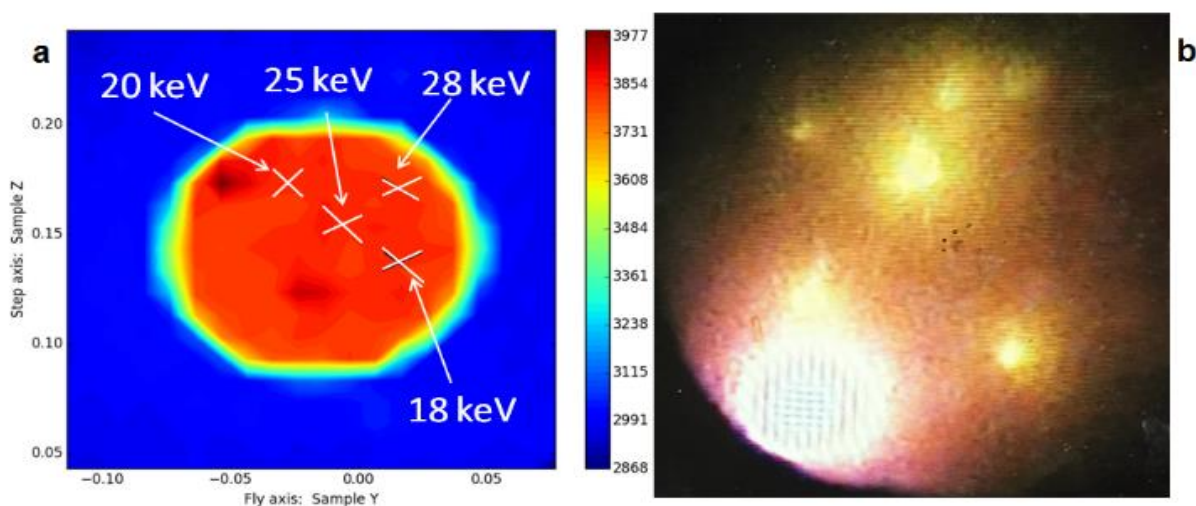


Figure 3. (a) X-ray tomography of a sample of SrC_2O_4 showing the regions of X-ray irradiation within the sample. Locations marked with an “x” indicate regions that were irradiated at the specified energy. (b) Visual evidence of laser-induced fluorescence within the irradiated regions (yellow spots) from the same sample shown in (a). The photo was taken as viewed in a DAC looking through one of the diamonds via a microscope. This figure is reproduced from reference 48.

Results and Analysis

Energy Dependence

Visual evidence of the X-ray induced modification of SrC_2O_4 at various energies is presented in figure 3. Figure 4a displays diffraction patterns of SrC_2O_4 irradiated with 20 keV X-rays as a function of the time of irradiation. The initial pattern is shown in black, and the subsequent patterns are stacked according to increasing time of irradiation. The integrated area of all diffraction peaks reduce as the time of irradiation increases. This symmetric decrease across all peaks is evidence of loss of crystallinity.^{12, 46, 47,}

⁴⁹ We suspect that X-ray induced decomposition of strontium oxalate and subsequent synthesis of CO-derived material causes the observed loss of crystallinity. Thus, quantifying loss of crystallinity provides a barometer to determine the energy dependence of x-ray induced synthesis of CO-derived material from irradiation of SrC_2O_4 . To quantify the loss of crystallinity as a function of time we analyze the changing

integrated area of the strongest diffraction peak (highlighted in figure 4a). Principally, any peak could be chosen, and the results would not be affected, but we chose the peak with the highest intensity because it provides the best signal to noise ratio and thus minimizes any random noise in the data. The chosen peak corresponds to the red diffraction plane indicated in figure 4b.

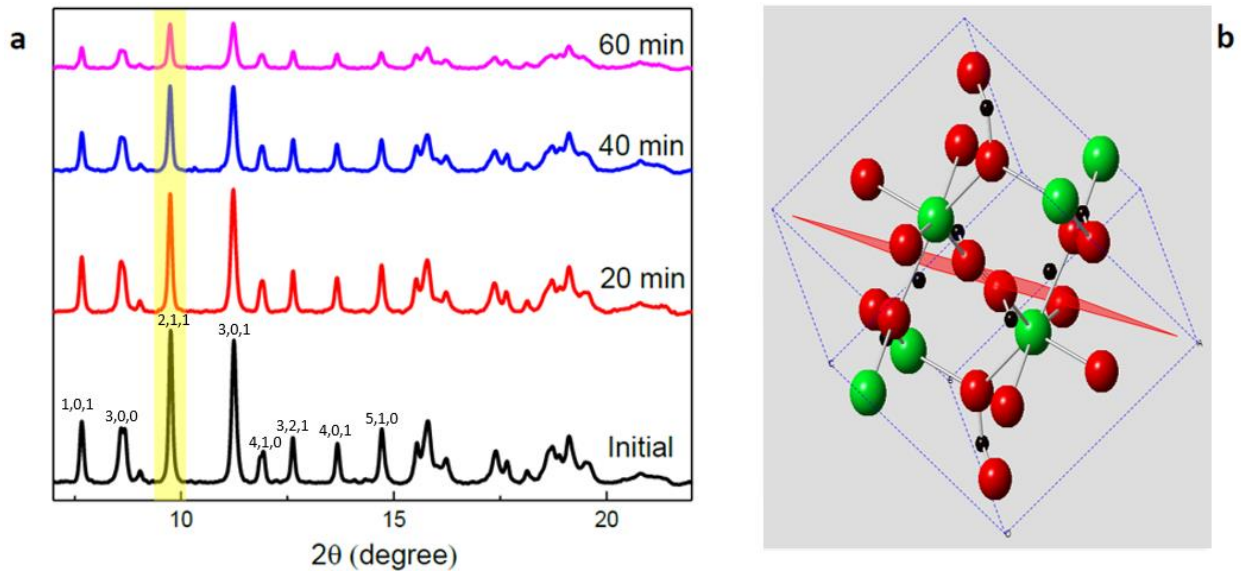


Figure 4. (a) Diffraction patterns of SrC₂O₄ at ambient conditions as a function of time of irradiation with 20 keV X-rays. Diffraction peaks are labeled with corresponding Miller indices. **(b)** representation of the unit cell of SrC₂O₄^{50, 51} which has tetragonal structure and lattice parameters: $a = b = 12.29$, $c = 5.01$ Å. The red plane ($h=2$, $k=1$, $l=1$) shown closely correlated to the d-spacing of the peak highlighted in **(a)**. the representation of the unit cell in **(b)** was produced with the CrystalMaker® Software package.⁵² This figure is reproduced from reference 48.

To quantify X-ray induced loss of crystallinity as a function of time we define the Loss of Crystallinity (LoC) as:

$$\text{LoC}(t) = 1 - \frac{A_t}{A_{t=0}} \quad (3)$$

where A_t and $A_{t=0}$ are respectively the areas of the highlighted peak at time t and at time $t = 0$ as shown in figure 4a. The LoC as a function of time, for each of the studied energies, is presented in figure 5. To ensure that any variation in the reported LoC are indicative of differences caused by irradiating with photons of different energy, the LoCs are normalized based on the photon flux and area of irradiation.

To determine the kinetics of the process we analyzed the loss of crystallinity in the frame of the Avrami Model as:⁵³

$$\text{LoC}(t) = \text{LoC}_\infty(1 - \exp(-(k t)^n)) \quad (4)$$

where $\text{LoC}(t)$ and LoC_∞ are the LoC at time t and at the end of the process, k is the rate constant, and n is a parameter whose value depends on the geometry of the process. Note that the kinetics of the loss of crystallinity may not accurately represent the kinetics of the synthesis reaction, but it still provides valuable information. Originally, the Avrami equation was proposed to model crystal growth from the liquid phase^{53, 54} and later has been adapted to the polymerization process.⁵⁵⁻⁵⁷ Since the product of the reaction is similar to PCO, we expect that the kinetics of the loss of crystallinity should be similar to the kinetics of a polymerization process and thus the Avrami model gives physically relevant information about the process. Other studies of radiation damage often characterize the kinetics of damage by fitting to an exponential function.^{58, 59} The Avrami model is like an exponential function, but it includes an additional parameter, n , which improves the fits to our data and provides additional information about the dimensionality of the process. Figure 5 displays $\text{LoC}(t)$ for the studied energies and the lines of best fit from equation 4. Values of k , n , and LoC_∞ obtained from the fit are supplied in Table 1 for each energy. The three parameter fits appear to follow the data relatively well, and they give physically reasonable values for each of the fit parameters.

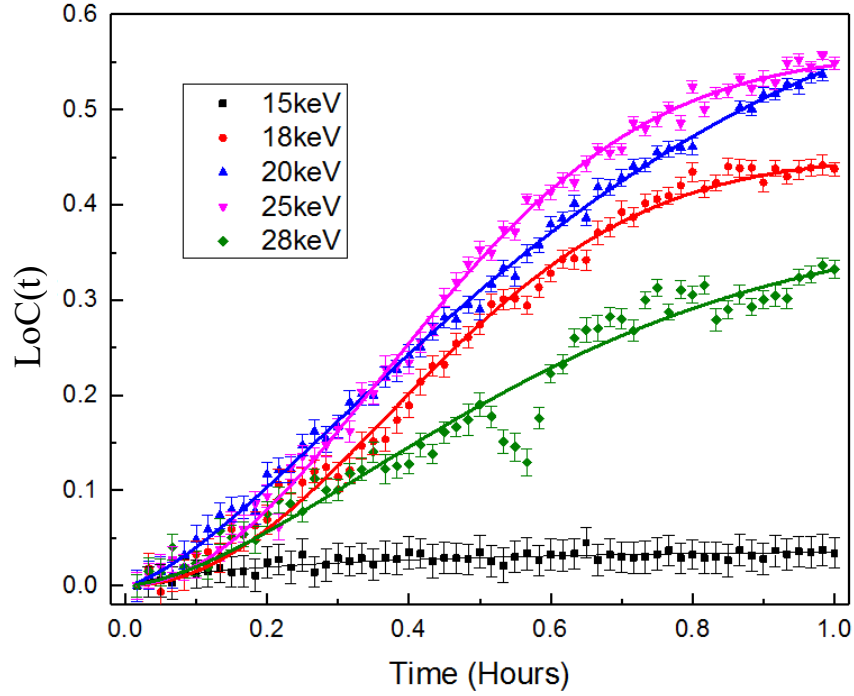


Figure 5. Displays the kinetics of the x-ray induced loss of crystallinity of SrC_2O_4 at ambient conditions irradiated with X-rays of various energies. The solid lines are fit to the Avrami model, equation (4), and the corresponding fit parameters are presented in table 1. This figure is reproduced from reference 48.

Table 1. Avrami model parameters k , n , and LoC_∞ obtained from the fit of SrC_2O_4 loss of crystallinity kinetics measured at ambient conditions and different X-rays energies. This table is reproduced from reference 48.

Energy (keV)	$k(\text{h}^{-1})$	n	LoC_∞
15.0	4.7 ± 0.5	1.1 ± 0.17	0.033 ± 0.012
18.0	1.89 ± 0.03	1.97 ± 0.06	0.46 ± 0.006
20.0	1.42 ± 0.05	1.4 ± 0.3	0.67 ± 0.018
25.0	1.90 ± 0.02	1.91 ± 0.05	0.57 ± 0.006
28.0	1.4 ± 0.2	1.5 ± 0.14	0.42 ± 0.05

Irradiating for one hour is not long enough to reach the maximum loss of crystallinity, LoC_{∞} , for most of the energies studied. This is evident in figure 5 as most LoC traces have non-zero slope after an hour of irradiation. One of the primary goals in the experiment is to produce the maximum amount of CO-derived material. We suspect that maximum CO-derived material is produced when maximum loss of crystallinity is observed. Thus, we are particularly interested in determining LoC_{∞} . By fitting the data with the Avrami model we can infer LoC_{∞} for all energies despite the limited time of irradiation.

Generally, the k parameters obtained from the fits show that the rate of loss of crystallinity varies by about 35%, and it appears to be unrelated to the final loss of crystallinity. The 15 keV trace is the exception. For that fit, the k value is significantly larger than the others, but that trace also yields almost no loss of crystallinity. The anomalous behavior of the 15keV trace is discussed further below. As shown in table 1, irradiating with 20 keV X-rays induces the maximum final loss of crystallinity though the rate of loss is nearly the same as that when irradiating with 28 keV X-rays, which produced significantly lower final loss of crystallinity. The n values obtained from the fit are all between 1 and 2, which indicates that the geometry of the process is linear according to the Avrami equation.⁶⁰ In other words, the n values from the fit suggest that crystallinity loss only occurs in the path of the X-ray beam, which is as expected.

Figure 6 shows the final loss of crystallinity, LoC_{∞} , as determined by the best fit lines displayed in figure 5, versus the energy of the irradiating X-ray beam. The inset in the figure shows the average ion chamber current for each of the studied energies. The ion chamber current is proportional to the photon flux which is important to consider in combination with the obtained LoC_{∞} values. Irradiating with 15 keV X-rays achieves very little LoC. Increasing X-ray energy leads to dramatically increased LoC_{∞} with a maximum at 20 keV. Increasing X-ray energy beyond 20 keV leads to slow decrease of LoC_{∞} .

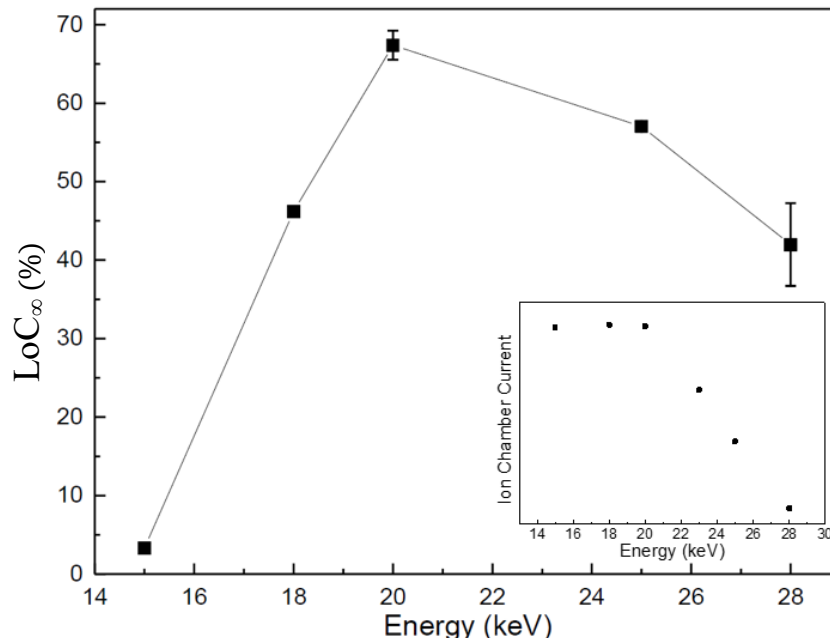


Figure 6. Final loss of crystallinity, LoC_{∞} , as a function of irradiating X-ray energy. The Inset shows ion chamber current recorded at each energy. The ion chamber current is proportional to the photon flux of the beam. This figure is reproduced from reference 48.

The observed energy dependence supports the notion that loss of crystallinity is triggered by X-ray induced excitation of K-shell electrons. When the molecule absorbs a sufficiently energetic X-ray photon, a K-shell electron is either promoted to a higher valence-like state or into the continuum.^{61, 62} The K-shell electron leaves behind a core-hole, which is extremely unstable. The core-hole state will rapidly decay by the Auger process or other radiative processes. Regardless of the exact decay mechanism, the strontium cation is left in an unstable higher charge state, which drives molecular dissociation. Similar mechanisms were observed in the X-ray-induced ionization of molecular N_2 ^{61, 62} and dissociation of XeF_2 .⁶³

In our experiment, the absorption of a sufficiently energetic X-ray photon leads to a change of the oxidation state of the strontium cation, from Sr^{2+} to Sr^{2+x} . The Sr^{2+x} cation then attracts one or more (x) electrons from the electron-rich $C_2O_4^{2-}$ anion to refill the vacancies induced by the photon absorption. This process destabilizes the newly electron-deficient $C_2O_4^{2-(x)}$ which breaks apart to enable formation of the

novel CO-derived material. The fact that little or no loss of crystallinity is observed when irradiating below strontium's K-edge of 16.1 keV strongly indicates that the X-ray induced loss of crystallinity is only triggered by the excitation of a K-shell electron. Additionally, our data suggests that secondary processes are important to optimizing the loss of crystallinity and possibly to increasing the amount of material synthesized. We observe the maximum loss of crystallinity when irradiating with 20 keV X-rays, a few keV above the Sr K-edge. When strontium absorbs a photon of energy greater than its K-edge, the extra energy will lead to the emission of a K-shell electron with significant kinetic energy, called a photoelectron. The photoelectron likely causes secondary radiation damage, and we suspect the emission of photoelectrons is responsible for the increased loss of crystallinity observed above the Sr K-edge. Future experiments will aim to clarify the cationic dependence of X-ray induced loss of crystallinity.

Pressure Dependence

We used the same experimental system and similar analysis techniques to examine the pressure dependence of X-ray induced modifications of SrC₂O₄. Based on the preliminary result from the energy dependence study, which suggested that 20 keV X-rays achieved maximum loss of crystallinity, we elected to set the energy of X-ray beam at 20 keV. Then we irradiated unique locations within a fresh sample, while increasing pressure and attempting to obtain Raman spectra from the damaged material between each subsequent irradiation. Figure 7 shows initial diffraction patterns at selected pressures starting with ambient pressure and reaching a maximum of 7.6 GPa. Changes of the initial diffractograms suggest that the SrC₂O₄ crystal lattice gets distorted upon compression. We observe dramatic pressure induced changes somewhere in the 0-2 GPa range and additional changes above 4 GPa. These changes are likely due to one or more structural phase transitions of SrC₂O₄, and future studies aim to confirm these phase transitions.

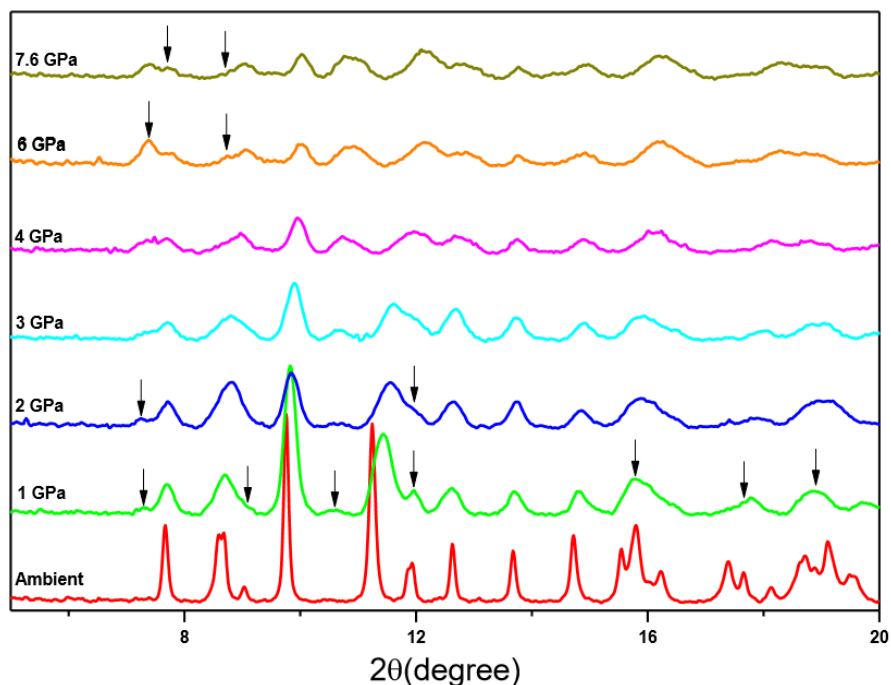


Figure 7. Initial diffractograms of SrC_2O_4 for each of the studied pressures. Features marked with black arrows highlight possible evidence of pressure-induced structural changes. This figure is reproduced from reference 48.

The initial diffractograms give information about pressure-induced changes, but to analyze X-ray-induced changes we used the same method as in the energy dependence study. Namely, we obtained the loss of crystallinity as a function of time, $\text{LoC}(t)$, by analyzing the changing area of the (2,1,1) diffraction peak (highlighted area in Figure 4a), according to equation 3. Figure 8 displays the $\text{LoC}(t)$ for selected pressures.

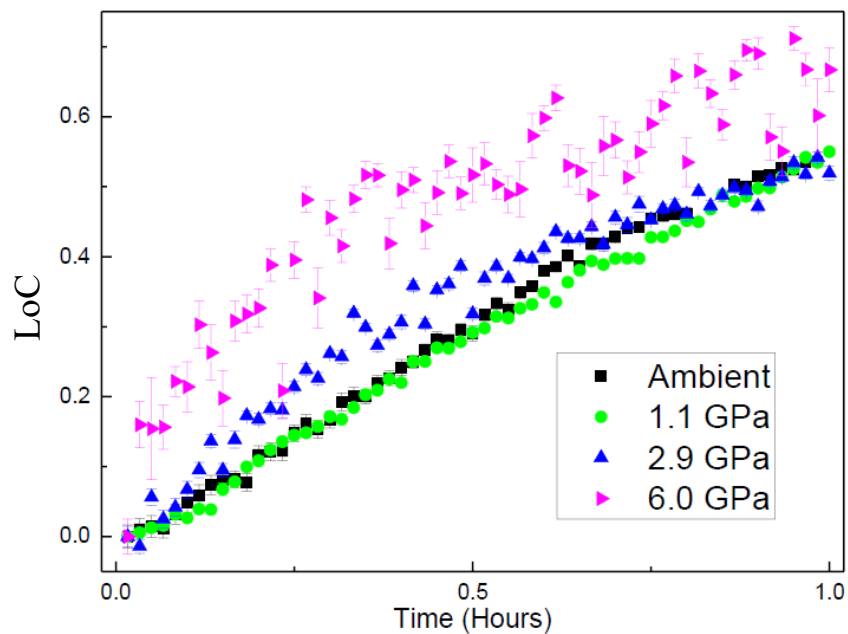


Figure 8. Kinetics of loss of SrC₂O₄ crystallinity at selected pressures irradiated with 20 keV X-rays. This figure is reproduced from reference 48.

As for the energy dependence, the kinetics of the loss of crystallinity can be analyzed in the frame of the Avrami model, equation 4. The fit values of k , n , and the maximum loss of crystallinity, LoC_{∞} , are given in Table 2 below.

Table 2. Avrami model parameters k , n , and LoC_{∞} obtained from fit of SrC_2O_4 loss of crystallinity kinetics at various pressures under irradiation of 20 keV X-rays. This table is reproduced from reference 48.

Pressure (GPa)	$k(h^{-1})$	n	LoC_{∞}
Ambient	1.42 ± 0.05	1.43 ± 0.03	0.67 ± 0.02
1	0.9 ± 0.11	1.23 ± 0.04	0.96 ± 0.09
2	2.1 ± 0.14	1.4 ± 0.11	0.51 ± 0.02
3	2.0 ± 0.17	1.12 ± 0.07	0.59 ± 0.03
4	1.6 ± 0.4	0.94 ± 0.09	0.67 ± 0.08
6	2.5 ± 0.8	0.7 ± 0.11	0.78 ± 0.09
7.6	2.4 ± 0.2	1.6 ± 0.2	0.54 ± 0.03

The k parameters determined from the fits show that changing sample pressure dramatically effects the rate of loss of crystallinity. The rate initially decreases as the sample is compressed from ambient pressure to 1 GPa, but then it increases dramatically, though not monotonically, as pressure increases from 1 GPa to 6 GPa. There appears to be a complicated dependence of the rate of loss on sample pressure. The n values obtained from the fit are between 0.7 and 2 for all studied pressures, which again indicates that the geometry of the process is linear, as expected. Once more, the final loss of crystallinity at various pressures is of particular interest, so those values are plotted as a function of pressure in figure 9 below.

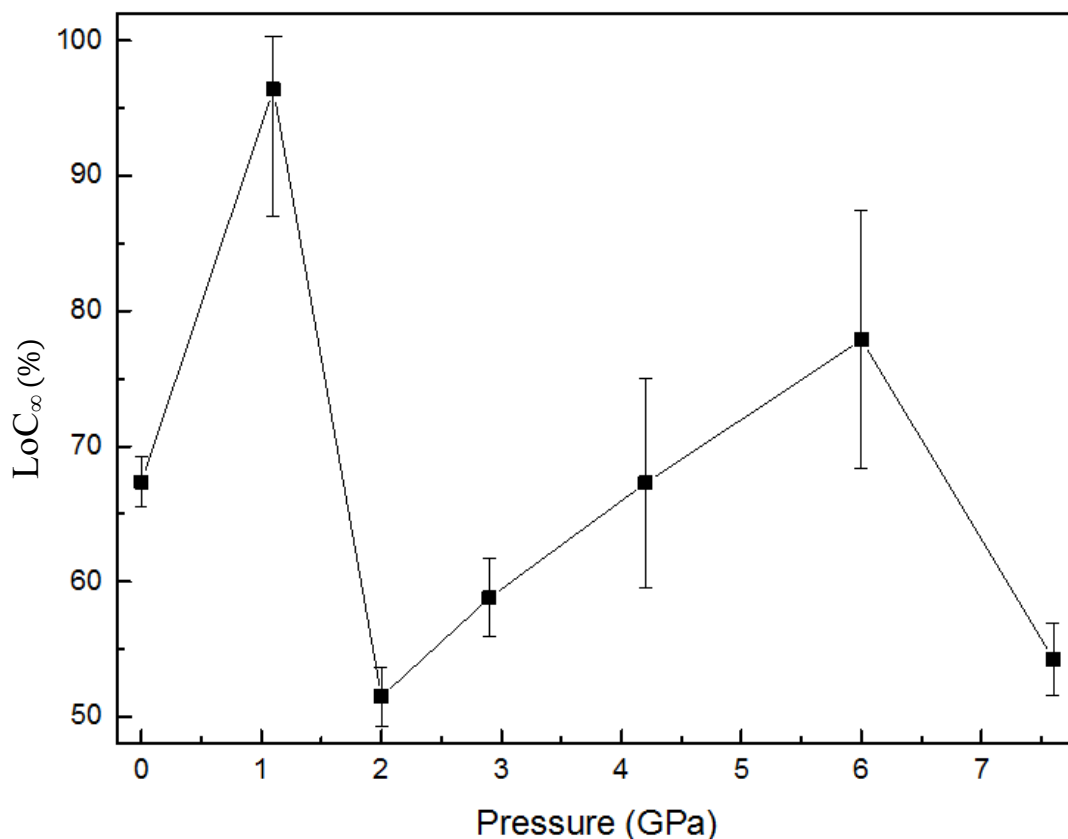


Figure 9. Final loss of crystallinity, LoC_{∞} , as a function of pressure. This figure is reproduced from reference 48.

Figure 9 shows evidence that the loss of crystallinity depends strongly on the sample pressure. Increasing pressure from ambient to 1 GPa leads to a dramatic increase of LoC_{∞} from 67% to 96%. However, as pressure increases further, from 1 GPa to 2 GPa, the LoC_{∞} drops to 51%, below that achieved at ambient conditions. Further compression beyond 2 GPa leads to steady increase of LoC_{∞} , until a second local maximum of 78% is achieved at 6 GPa. Pressurizing from 6 to 7.6 GPa leads to another significant decrease of LoC_{∞} . These observations suggest that at least two competing factors govern the pressure dependence of X-ray-induced loss of crystallinity. On the one hand, we hypothesize that increasing pressure reduced distance between molecules. As the intermolecular distance decreases, coupling

between SrC_2O_4 units increases and the ionic bond between the cation and anion gets stronger. Presumably, when the coupling between the cation and anion increases, less energy is required to transfer an electron from the anion to refill vacancies in the cation. Thus, charge transfer is facilitated by increased pressure, which in turn enhances the X-ray induced loss of SrC_2O_4 crystallinity and leads to greater production of CO-derived material. However, if this were the only effect from increasing pressure, we would expect a monotonic increase in the final loss of crystallinity with increased pressure. We further hypothesize that the pressure-induced distortion of the SrC_2O_4 crystalline structure, as evident in figure 7, reduce the efficiency of charge transfer and leading to decreased final loss of crystallinity. Similar dependence of the decomposition rate on the sample pressure was observed in prior studies of TATB,⁴⁶ ⁴⁹ KClO_3 ,⁴⁷ and KClO_4 .¹² For KClO_3 , a dramatic drop in the decomposition rate when the sample was observed when the sample was pressurized above 1.5 GPa.⁴⁷ That drop was attributed to a phase transition, and the phenomena was termed: *Phase-dependent decomposition*.

Summary and Conclusions

The work presented in this chapter of the thesis, represents the first reported systematic studies of the energy and high-pressure dependence of X-ray induced modifications of crystalline strontium oxalate. Recall that our experiments had two primary goals: first to find the optimal conditions for X-ray induced synthesis of CO-derived material from irradiation of strontium oxalate, and second to provide general insight into the energy and pressure dependence of X-ray induced photochemical reactions. We found that irradiating SrC_2O_4 with 20 keV X-rays achieves the greatest loss of crystallinity and that by pressurizing the sample to about 1 GPa and irradiating with 20 keV X-rays a maximum final loss of crystallinity of 96% is attainable. These parameters, 20 keV X-ray energy and 1 GPa sample pressure, likely represent the optimal conditions for X-ray induced synthesis of CO-derived material from irradiation of SrC_2O_4 . Future studies will be required to refine these conditions and truly optimize the X-ray induced

reaction, but these results indicate that such optimization is achievable. While X-ray induced photochemical reactions are unique, some of the results from this work point to generally applicable energy and pressure dependencies of photochemical processes.

The results from this study provide insight into the general energy and pressure dependence of X-ray induced photochemical reactions. For example, we found that excitation of a k-shell electron triggers the loss of crystallinity, which suggests that other X-ray induced reactions may be initiated similarly. This implies that X-ray induced reactions may only occur if the incident photon is sufficiently energetic to excite a K-shell electron from the cation. Which in turn implies a cationic dependence of X-ray induced photochemical reactions. Further studies (like the NO_3 study presented in the following chapter) will aim to corroborate this apparent cationic dependence. Additionally, we found that pressurizing the sample environment has dramatic effects on the rate of loss and the final loss of crystallinity. We hypothesized that compressing materials generally increases cation-anion coupling, facilitating charge transfer, and thus increasing the final loss of crystallinity, except when pressurization induces structural changes that retard charge transfer. This result verifies similar results reported for other X-ray induced photochemical reactions.

Chapter 3 – Barium and Strontium Nitrate

Introduction

In 1958, a pair of researchers from Queen’s University of Belfast performed a study on the X-ray induced decomposition of various alkali nitrates including barium and strontium nitrate ($\text{Ba}(\text{NO}_3)_2$ and $\text{Sr}(\text{NO}_3)_2$ respectively).⁶⁴ They found that, in all cases, irradiation caused the nitrate anion to decompose into nitrite and oxygen gas, according to the photochemical reaction:



This early study of X-ray photochemistry identified the reaction products and attempted to quantify them, but the experimental conditions were significantly different from those that are common today. In particular, the photon flux of the X-ray source was significantly less than the photon flux produced by modern X-ray sources. There is evidence, particularly from X-ray free electron laser (XFEL) experiments, that radiation damage induced by high photon flux radiation, differs greatly from that induced at low flux.⁶⁵ Nevertheless, the 1958 study inspired us to perform similar experiments in which we irradiated strontium and barium nitrate with monochromatic X-rays of various energies and examined the decomposition reaction with ADXRD and Raman spectroscopy. By comparing X-ray induced damage of strontium and barium nitrate, we hope to elucidate the expected cationic dependence of X-ray induced damage as hypothesized from the energy dependence of X-ray-induced modifications of SrC_2O_4 . Additionally, by identifying the reaction products we can corroborate the results of the 1958 study. Note that the work presented in this section of the thesis is also discussed in our publication entitled *Cationic Dependence of X-ray-induced Damage in Strontium and Barium Nitrate*.⁶⁶

Barium and strontium nitrate are ideal materials for this study. Each has a simple cubic structure, space group $\text{Pa}\bar{3}$, with lattice constants 8.118 and 7.781 Å, respectively.⁶⁷ The unit cells of barium and strontium nitrate are displayed below in figure 10. Barium’s K-edge is 37.414 keV whereas strontium’s K-edge is 16.106 keV.⁶⁸ The probability of a nitrogen or oxygen atom interacting with an X-ray of ~16 keV or

37 keV is very low due to their small absorption cross sections at such high energies.⁶⁹ This aids in understanding the stimuli in these systems as we can assume that the primary interaction is between the X-rays and the heavy cations. It is known that interaction between X-rays and heavy cations triggers many possible electronic relaxation processes^{15, 70} that may lead to diverse results. By observing qualitative and quantitative differences between X-ray induced damage, we can offer insight into the general mechanism governing high photon flux X-ray induced damage of ionic solids and confirm the expected cationic dependence.

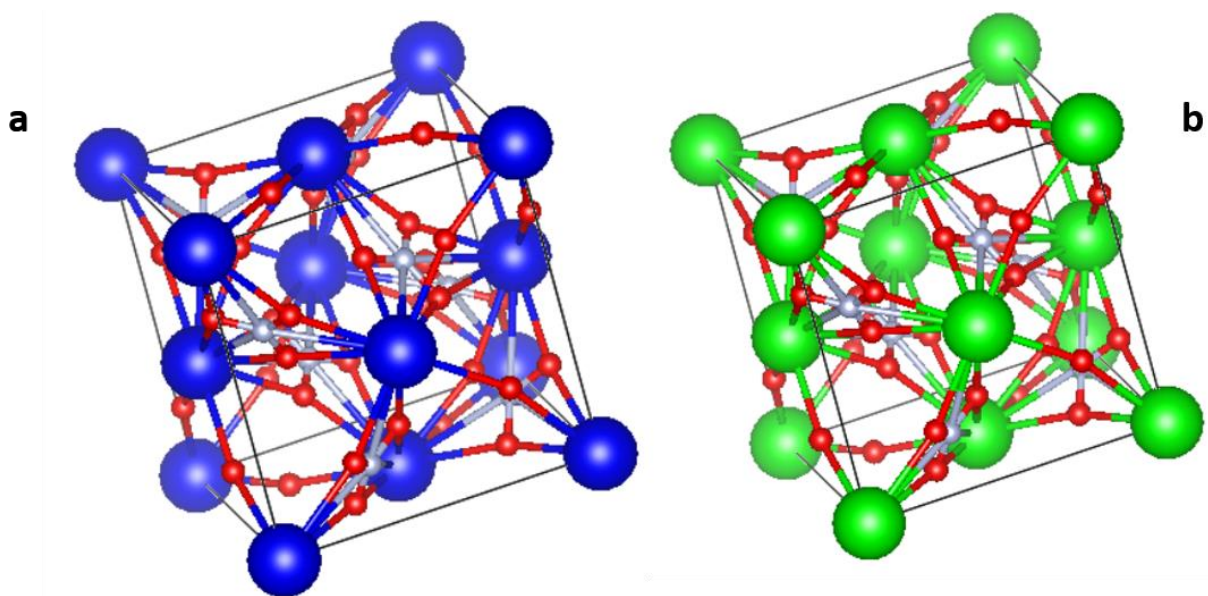


Figure 10. The unit cells of **(a)** barium and **(b)** strontium nitrate. Barium and strontium atoms are shown in blue and green respectively, while nitrogen is shown in grey and oxygen in red. Both materials exhibit simple cubic structure, space group $Pa\bar{3}$ with $Z=4$ formula units. The barium nitrate unit cell is slightly larger because its lattice constant, 8.118 \AA , is greater than that of strontium nitrate, 7.781 \AA .⁶⁷ These representations of unit cells were produced using the VESTA[®] program.⁷¹

Experiment

To investigate the cationic dependence of X-ray induced damage of barium and strontium nitrate, we performed two sets of similar experiments at the 16 BM-D beamline at APS. The DAC setup is similar to the setup for the strontium oxalate experiments, but extra precautions were taken due to the nature of the nitrate samples. Symmetric style DACs, with culets of 400-500 μm were used to provide a sealed, thermally conductive environment in which X-ray photochemistry could occur and be observed. Stainless-steel gaskets were indented to ~ 30 μm and sample chambers were drilled into the gaskets via the laser micro-machining system at APS.⁷² Unlike strontium oxalate, we expected the irradiation of the nitrate species to produce mobile gaseous species. As such, to ensure that our results were not influenced by previous studies, we performed each experiment on a fresh sample. However, due to the hydrophilic nature of barium and strontium nitrate, the DACs had to be loaded and sealed inside a glovebox filled with an inert atmosphere to ensure that samples were not exposed to atmospheric moisture. To expedite DAC loading in glovebox, gaskets were laser drilled with two or three sample chambers, each about 80 μm in diameter, as shown in figure 11. The sample chambers were symmetrically placed about the center of the diamond-diamond axis so that they pressurize similarly upon compression. A ruby sphere was loaded into each sample chamber for pressure measurements and no pressure transmitting medium was used. This DAC preparation is similar to that in reference 73 where a pressure difference of 10-20% was measured between sample chambers in the same gasket.⁷³ DACs were sealed and pressurized to about 0.5 GPa prior to irradiation. Some pressure variation ($< 10\%$) was observed between sample chambers.

The irradiating X-ray system, Raman system and data collection were also like those used for the strontium oxalate experiment. Since we were interested in the cationic dependence of X-ray induced damage, we used the 16 BM-D monochromator to select X-ray energies around the K-edges of the strontium and barium. An ion chamber placed directly upstream of the sample measured the photon flux

of the X-ray beam. These measurements were corrected based on diamond absorption to determine the incident photon flux. Samples, in separate sample chambers, were placed at the focus of the X-ray beam, and ADXRD patterns were collected with a MAR345[®] image plate detector once per minute over an hour of irradiation. The 2D diffraction patterns were reduced to a diffractogram using the Dioptas[®] program,³⁶ which were converted to intensity vs d-space plots via Bragg's law. The pre- and post-irradiation samples were characterized with in-situ Raman spectroscopy to determine the nature of reaction products.

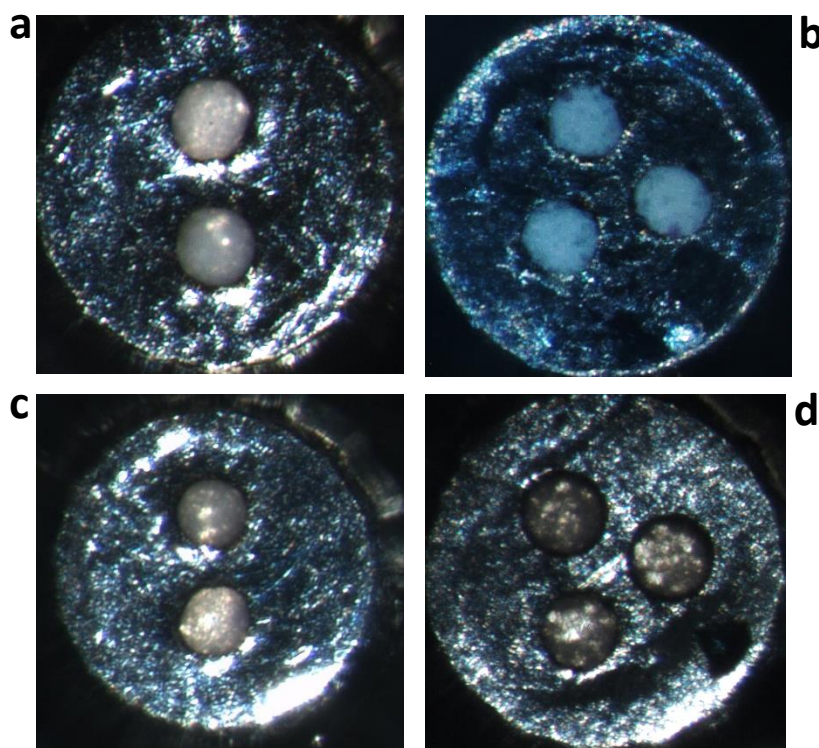


Figure 11. Samples of barium nitrate loaded in stainless-steel gaskets prepared as described above. **(a, b)** Samples pressurized in DAC, before irradiation, **(c)** pressurized in DAC after an hour of irradiation at 34 keV (top) and 36 keV (bottom), **(d)** after an hour of irradiation at 38, 40, and 42 keV (clockwise from top left). Note the dark tint of the samples that were irradiated at higher energy. This figure is reproduced from reference 66.

Results and Analysis

Visual Evidence

Figure 11 presents pictures of samples of barium nitrate in DAC before and after irradiation at various energies. The pictures were taken via an optical microscope looking through one of the diamonds of a sealed DAC. The samples irradiated with higher energy X-ray photons (i.e. above the Ba K-edge) appear with a brown/dark tint, but no such change is observed at lower energies. The visible change is the first evidence of an X-ray driven photochemical reaction. The lack of visible change in the samples irradiated with lower energy X-rays suggests a bifurcation of photochemical reactions induced by high and low energy X-rays, where high and low are determined with respect to the K-edge of the cation in the irradiated sample. The Raman spectra of pre- and post-irradiation samples further elucidates this bifurcation.

Raman Spectroscopy

Selected in-situ Raman spectra of pre- and post-irradiation samples of barium and strontium nitrate are presented in figure 12. The pre-irradiation spectra of barium and strontium nitrate are similar. Both spectra exhibit strong peaks at ~ 745 and ~ 1055 cm^{-1} and a small shoulder at ~ 1400 cm^{-1} on the diamond peak (1332 cm^{-1}). These features are in good agreement with previously reported spectra of these materials.^{74, 75} The Raman modes correspond to the in-plane bend, the symmetric stretch, and the antisymmetric stretch of the NO_3^- anion respectively. Post-irradiation Raman spectra exhibit slight but critical differences in comparison to pre-irradiation spectra.

The post-irradiation spectra of barium and strontium nitrate samples irradiated with higher energy (above-K-edge) X-rays show new peaks that are much less apparent or non-existent in the low energy (below-K-edge) Raman spectra. When present, the new peaks appear at ~ 840 and ~ 1560 cm^{-1} . The new peak near 840 cm^{-1} can be assigned to the O-O stretch mode in a mixture of MO_2 and MO ($M = \text{Ba}$ or

Sr)⁷⁵ or to the bending mode of NO₂⁻.⁶⁴ The new peak around ~1560 cm⁻¹ can be assigned to the well-known O-O vibrational stretch mode in O₂.⁷⁶ The appearance of these new Raman modes corroborates the previously proposed X-ray induced decomposition of the nitrate anion into nitrite and oxygen gas.⁶⁴ The decomposition of the nitrate anion likely leaves the molecular system in an unstable, highly-energetic state. Various relaxation channels may lead to the formation of multiple molecular species including NO₂, O₂, MO, and MO₂, etc. which could not be distinguished based on Raman spectroscopy. However, the brown/dark tint of some post-irradiation samples suggests that NO₂ gas is likely produced.

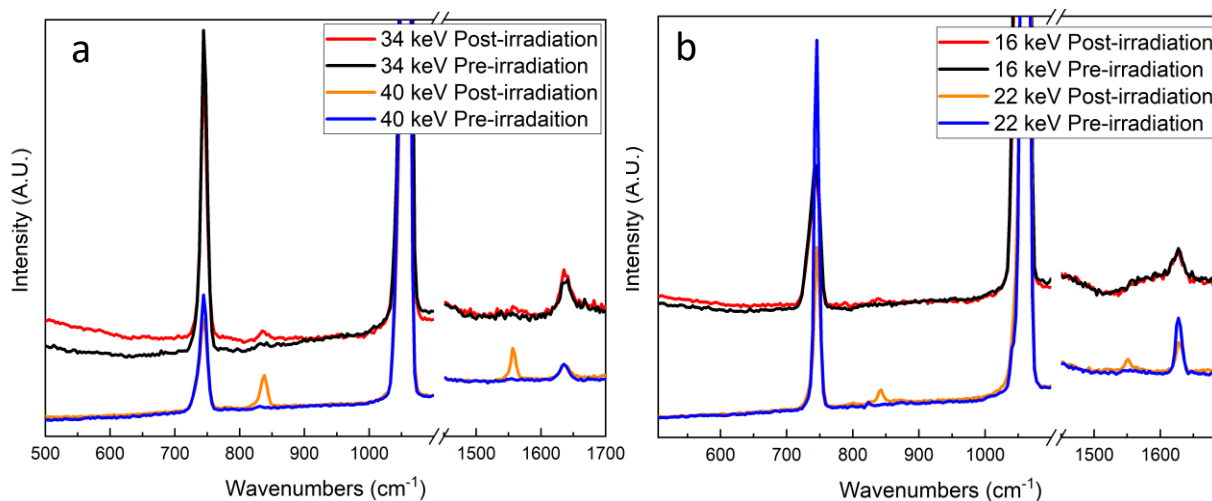


Figure 12. Pre- and post-irradiation Raman spectra of **(a)** barium and **(b)** strontium nitrate. Note the appearance of new peaks in the higher-energy, post-irradiation spectra. This figure is reproduced from reference 66.

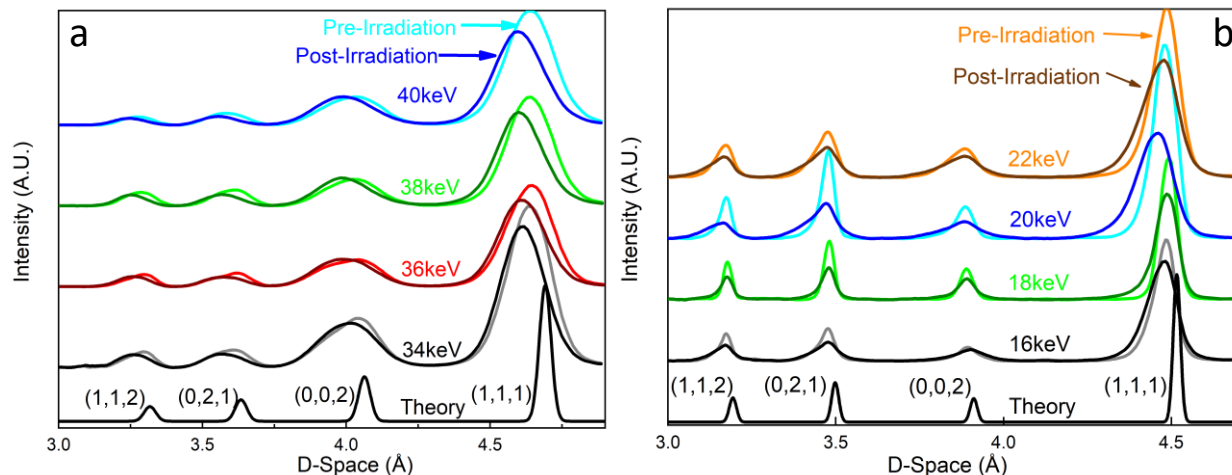


Figure 13. Pre- and post-irradiation diffraction patterns of **(a)** barium and **(b)** strontium nitrate. Patterns are stacked and colored by energy, and light colors indicate pre-irradiation patterns while dark colors indicate post-irradiation patterns. We observe three qualitative changes of peaks in diffraction patterns: integrated area changes, peak center shifts, and peak width changes. This figure is reproduced from reference 66.

X-ray Diffraction

Pre- and post-irradiation diffractograms of (a) barium and (b) strontium nitrate irradiated with X-rays of various energy are presented in figure 13. The shift of pre-irradiation diffraction peaks relative to theoretical peaks indicates that the samples are pressurized. The shifts are relatively small ($\sim 1\%$), and similar for all unique samples, which suggests that the various sample chambers are stressed to similarly modest pressures. Comparison of theoretical and experimental diffraction patterns provides information about the initial conditions of our samples, while comparison of the pre- and post-irradiation diffractograms offers information about X-ray induced changes.

Subtle alterations of the post-irradiation diffractograms are apparent when they are compared to their pre-irradiation counterparts. These alterations point to X-ray induced physical changes of the sample. Diffraction peak's integrated area, center, and full width at half maximum (FWHM), all evolve over the course of irradiation. However, the evolution of these parameters depends on the irradiating

photon energy and on the sample itself. Quantifying these differences gives further insight into the X-ray induced photochemical processes at work in each system at various energies.

To accurately compare the evolution of parameters of diffraction peaks obtained by irradiation of samples with subtly different geometries and X-ray beams of different energies and photon fluxes, data must be normalized carefully. We start by fitting each clearly distinguishable peak in a diffractogram to a Gaussian. Then we extract the integrated area, FWHM, peak center and error for each of these parameters from the fits. Each parameter is normalized to its initial value for a given peak at a given energy, and the percent change is presented as a function of fluence as:

$$\text{"%Change of X"(F)} \equiv 100\% \left(\frac{X(F)}{X(0)} - 1 \right) \quad (6)$$

Fluence, F , is defined as the total number of incident photons, and we calculate it as the product of photon flux and time of irradiation. Since the photon flux of the X-ray beam varies with energy, the total fluence after an hour of irradiation differs from sample to sample. To accurately compare, we separately truncated the barium and strontium data sets to the lowest total fluence after an hour of irradiation. The data sets were truncated at 4×10^9 and 9×10^9 Photons/ $(\mu\text{m})^2$ for barium and strontium respectively. Note that the total fluence of the strontium data sets was about twice that of barium.

As discussed in chapter 2, we propose that diminishing integrated area of diffraction peaks upon X-ray irradiation is indicative of X-ray induced loss of crystallinity. As the nitrate anion decomposes it induces atomic dislocations in the crystal lattice which reduce diffraction signal. The decomposition also leaves the molecular system in an unstable state, triggering relaxation processes that may induce additional atomic dislocations and further reduce diffraction signal. We quantify the loss of crystallinity (LoC) of our samples based on the changing integrated area of a diffraction peak as:

$$\text{LoC}(F) = 100\% \left(1 - \frac{\text{Peak Area}(F)}{\text{Peak Area}(0)} \right) \quad (7)$$

we calculate the LoC for selected diffraction peaks and then average them to obtain the results presented in figure 14. One surprising aspect of these results is that in some cases the initial average LoC as calculated in equation 7 yields negative values of LoC. These results appear unphysical as there is no physical mechanism for growth (negative loss) of crystallinity upon irradiation, but we interpret them as indicative of X-ray induced relaxation of uniaxial strain introduced by the initial pressurization of the samples. Such relaxation leads to reordering of atoms in the crystalline lattice which increases diffraction signal and produces negative LoC.

The results shown in figure 13 give valuable information about the X-ray induced photochemical processes at work. Below-k-edge (34 keV and 36 keV) irradiation of barium nitrate leads to initial decrease of the average LoC to slightly negative values, followed by modest increase to LoC of about 5%. This observation suggests that there are two competing X-ray induced processes that affect LoC: decomposition and relaxation of strain. The interplay of these two processes is clear in the oscillations of LoC at all energies. Interestingly, it is also apparent in the LoC of strontium oxalate presented in figures 5 and 8, though it was not recognized upon initial analysis of that data. Above-K-edge irradiation of barium leads to more dramatic increase of LoC to about 10%. The results for strontium nitrate are similar. Below-k-edge irradiation leads to modest LoC (~5%) while above-K-edge irradiation leads to significantly greater LoC. Both systems show that LoC increases when the irradiating photon energy is greater than the K-edge of the cation which is in good agreement with the results presented in chapter 2.

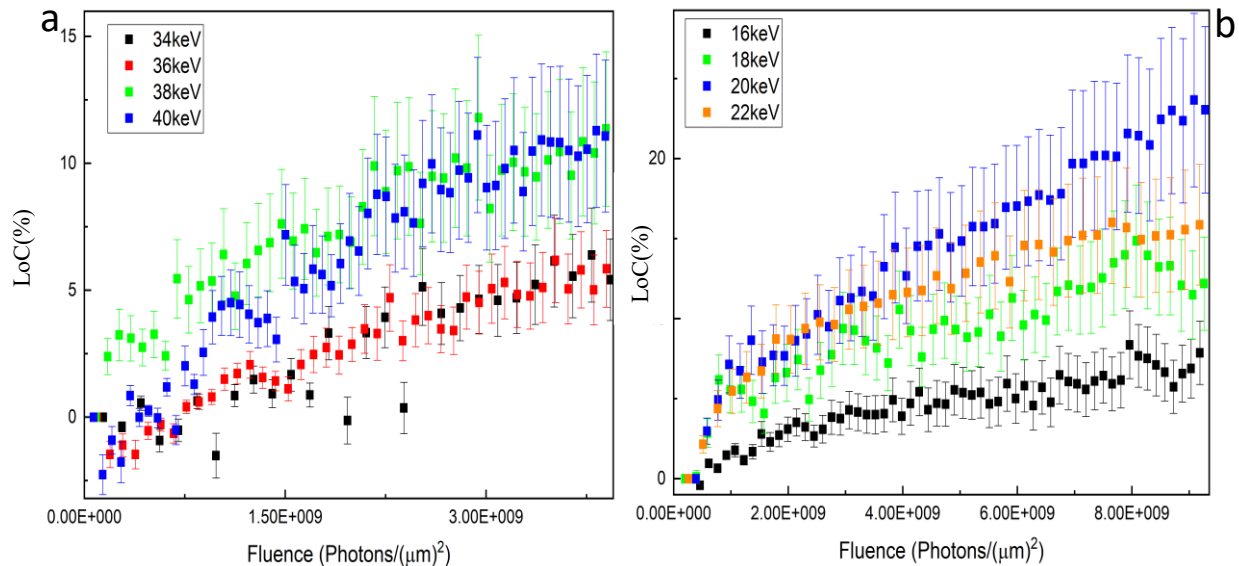


Figure 14. The average loss of crystallinity as a function of fluence for **(a)** barium and **(b)** strontium nitrate. The average is taken over selected peaks and the error bars indicate the standard deviation of the average. This figure is reproduced from reference 66.

The changing FWHM of diffraction peaks upon irradiation provides further insight to the X-ray induced processes at work. As discussed in chapter 1, factors that cause broadening of diffraction peaks are generally divided into two categories: instrumental and sample broadening contributions. The 16 BM-D system and consistency of data collection ensure that the instrumental contributions to peak broadening are small (< 1%) and constant at each energy.⁷⁷ Our normalization routine ensures that any observed broadening of diffraction peaks is caused by X-ray induced structural changes. Sample contributions to diffraction peak broadening are further categorized as size broadening of strain broadening factors.⁷⁸ In simple terms, samples composed of small crystalline grains and crystals that exhibit inhomogeneous strain will give broader diffraction patterns. X-ray induced increase of diffraction peak's FWHM indicates either decreasing grain size or increasing homogeneous strain. While decreasing FWHM indicates relaxation of inhomogeneous strain or grain size growth.

The irradiation induced changes of FWHM differ greatly in the two systems studied. Figure 15 displays the average changes of FWHM of (a) barium and (b) strontium as functions of fluence. In Barium nitrate below-k-edge irradiation leads to slight increase of FWHM (~5%), while above-K-edge irradiation leads to modest decrease of FWHM (~3%). In strontium, irradiation leads to dramatic increase of FWHM (~20-40%) of peaks at all energies, except when irradiating with 20 keV X-rays which cause even more drastic increase of FWHM (~90%). Except for the 20 keV data set, the trend of changing FWHM is opposite that of DY. Samples that were more decomposed by irradiation at a given energy exhibited decreasing FWHM in Ba, and smaller magnitude increases of FWHM in Sr. This further indicates that X-ray irradiation simultaneously induces localized relaxation of strain and decomposition.

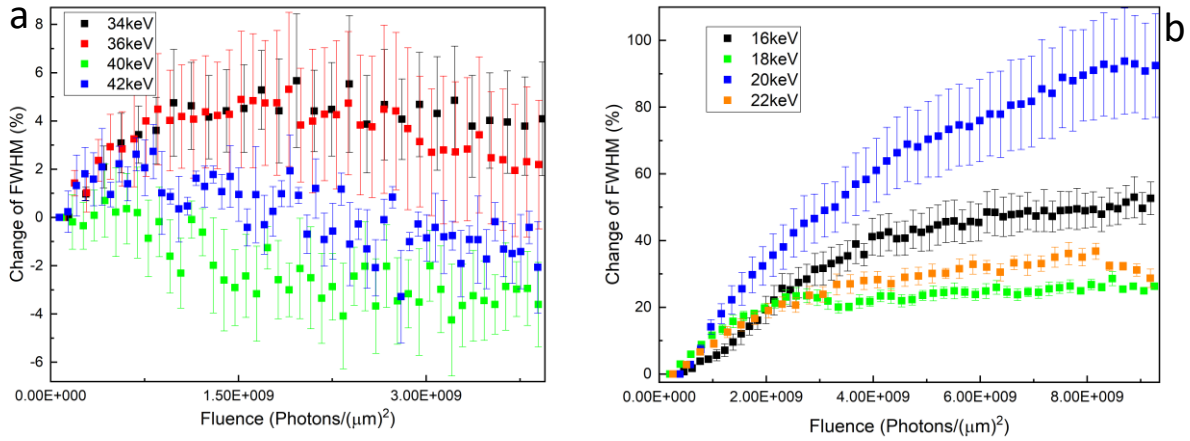


Figure 15. average percent change of full width at half maximum (FWHM) of peaks as a function of fluence for (a) barium and (b) strontium nitrate. The average is taken over selected peaks and the error bars indicate the standard deviation of the average. This figure is reproduced from reference 66.

The final changing parameter of diffraction peaks that we investigated was the shifts of diffraction peak's centers upon irradiation. Shifts of diffraction peaks are commonly attributed to homogeneous

strain,⁷⁸ which is characterized by changing unit cell lattice parameter(s). Due to the simple cubic structure of barium and strontium nitrate, their unit cells are fully characterized by one lattice parameter, a . For any cubic structure, the percent volume change of the unit cell can be calculated from the cubic d-spacing of a peak as:

$$\% \text{ Volume (F)} = 100\% \left(\frac{d(F)}{d(0)} \right)^3 \quad (8)$$

As for the other parameters analyzed, the change of unit cell volume is calculated for each peak and then averaged over selected peaks, as shown in figure 16 below. Upon irradiation, the unit cell of barium nitrate monotonically decreases regardless of X-ray energy, but the decrease is more dramatic for the above-K-edge irradiations. Interestingly the DY of barium nitrate, as presented in figure 13, followed a similar trend. Irradiation of strontium nitrate leads to more complex shifts of diffraction peaks. Initially irradiation leads to a slight increase of the volume of the unit cell of strontium nitrate, followed by more significant decrease. This effect is most apparent in the 16 keV data set, but it is noticeable for all energies. As for barium nitrate, above-K-edge irradiation of strontium nitrate leads to significantly greater reduction of unit cell volume as compared to below-K-edge irradiation. Presumably, the reduction of unit cell volume is caused by X-ray induced decomposition of the NO_3 anion and subsequent escape or rearrangement of reaction products. The trend of greater reduction of unit cell when irradiating with above-K-edge X-rays, then, corroborates the previous results.

Comparison of pre- and post-irradiation features of samples, as well as the evolution of diffraction peak parameters, elucidate the X-ray induced photochemical processes at work. Visual evidence, Raman spectroscopy, and ADXRD analysis demonstrate significant differences when irradiating above and below the target cation's K-edge. Darkening of samples irradiated above the K-edge suggests that the photochemical reaction proceeds differently above and below the K-edge of the target cation. This difference is supported by the observation that the above-K-edge post-irradiation Raman spectra exhibit

new peaks that are not apparent, or much less significant, in the below-K-edge post-irradiation spectra. Moreover, from ADXRD analysis we observe that above-K-edge irradiation leads to increased loss of crystallinity, and greater reduction of unit cell volumes. Altogether, these results corroborate the apparent k-edge dependence of X-ray induced photochemical reactions as initially proposed based on the energy dependence of X-ray induced modifications of strontium oxalate. However, our results also point to a more complicated X-ray induced photochemical process. Above-K-edge irradiation leads to reduction of FWHM in barium, and less significant increase of FWHM in strontium. Additionally, negative LoC was observed at low fluence. Combined, these observations suggest that interactions with X-rays simultaneously induce decomposition and relaxation of local strain

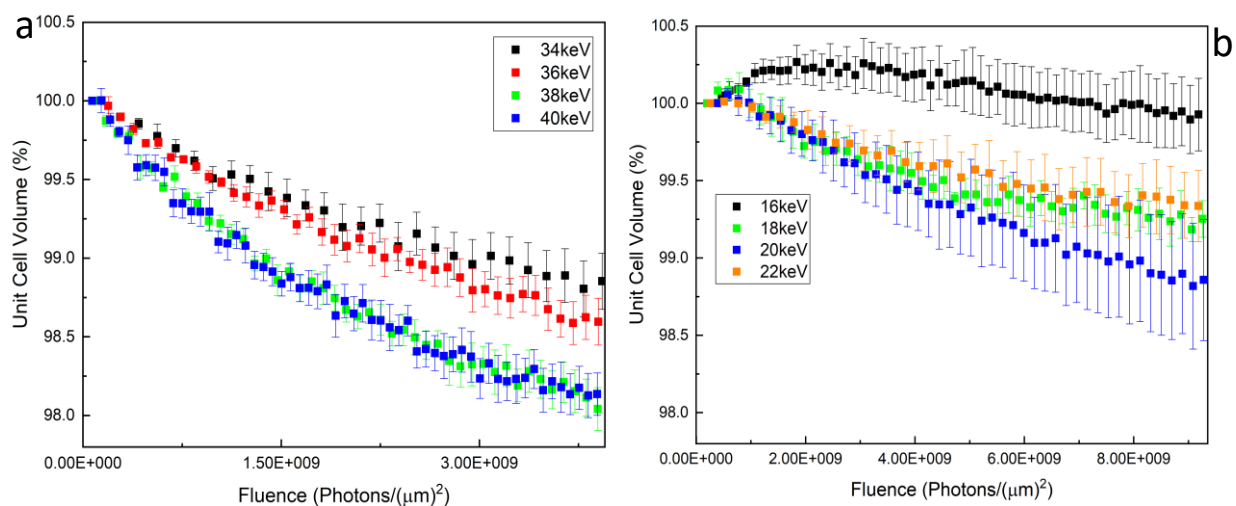


Figure 16. the average unit cell volume of (a) barium and (b) strontium nitrate as a function of fluence. The average is taken over selected peaks and the error bars indicate the standard deviation. This figure is reproduced from reference 66.

Comparison of the X-ray induced changes observed in barium and strontium nitrate elucidates the cationic dependence of X-ray induced photochemical reactions. In particular, the irradiation-stimulated evolution of the FWHM of diffraction peaks in barium and strontium nitrate differ considerably. These differences are shown in figure 14 and discussed above. We propose two plausible physical interpretations of this difference. Due to the differing size of barium and strontium, the unit cell packing of barium nitrate is less sensitive to the decomposition of the nitrate anion. In other words, because barium is larger, removal of the anion from the barium nitrate unit cell doesn't disturb the overall structure as much as removal from the strontium nitrate unit cell does. Thus, there is less buildup of inhomogeneous strain for barium nitrate which causes less change of FWHM. The dissimilarity of the absorption cross section of barium and strontium at their respective studied energies is an alternative physical driver of the observed difference. The likelihood of a strontium atom absorbing an 18 keV photon, is about twice that of a barium atom absorbing a 38 keV photon. Since our previous results indicate that absorption of a sufficiently energetic photon triggers loss of crystallinity, it is reasonable to suppose that a more absorbent cation will lead to a higher rate of damage. As decomposition and subsequent diffusion of reaction products leads to increased FWHM of diffraction peaks, the differing absorption cross section of the cations may be responsible for the observed difference of FWHM evolution in the two systems.

Summary and Conclusions

The experiments discussed in this chapter of the thesis had two major goals. First, to detect the products of X-ray induced decomposition of strontium and barium nitrate, and second, to identify any cationic dependence of the X-ray induced photochemical processes in these systems. Comparison of pre- and post-irradiation Raman spectroscopy, coupled with visual evidence, suggest that above-K-edge irradiation of both molecular species leads to the decomposition of the nitrate anion and production of NO₂ and O₂ gas. This result agrees with the 1958 study of these compounds. Interestingly, after Below-K-

edge irradiation, no signature of decomposition was detected visually or with Raman spectroscopy. The differences between above and below-K-edge irradiation were also investigated via ADXRD analysis. Loss of crystallinity, evolution of FWHM, and changes of unit cell volumes were calculated from gaussian fits to peaks in diffraction patterns obtained from irradiation at various energies. Generally, above-K-edge irradiation lead to greater loss of crystallinity, reduction or smaller-magnitude growth of FWHM, and increased reduction of unit cell volume. These results corroborate the K-edge dependence of X-ray induced decomposition of strontium oxalate discussed in chapter 2, but they also point to a second X-ray induced process that was not observed in the previous study. The initially negative loss of crystallinity, as well as the FWHM evolution observed in some data sets suggested that interaction with X-rays simultaneously triggers two competing process, i.e., decomposition and relaxation of local strain. Additionally, from comparison of the X-ray induced changes in strontium and barium nitrate, there is evidence that the cation's absorption cross section, and/or the packing efficiency of the molecular system, may play major roles in determining how X-ray photochemistry alters the system. This work represents another major step towards controlling X-ray photochemistry which is crucial to the developing field of useful hard X-ray photochemistry, as well as myriad related disciplines.

Chapter 4 – Conclusions and Future Work

The ubiquitous nature of X-ray photochemistry, coupled with the promising novel applications of X-rays in the developing field of useful hard X-ray photochemistry, make the optimization of X-ray photochemistry an important goal. X-ray damage has long been considered a nuisance as it complicates the use of X-rays in various fields. Finding parameters that can be manipulated to mitigate the effect of X-ray induced damage is critical to improved design of experimental systems that are currently limited by X-ray damage. More recently, X-ray photochemistry has been employed to drive various photochemical reactions, including novel synthesis and decomposition reactions like those discussed in this thesis. The utility of these new applications of X-ray photochemistry will be improved by optimizing the photochemical processes at work.

The work presented in this thesis represents foundational steps towards identifying parameters that can be manipulated to control X-ray induced photochemistry. In chapter two, we found the optimum X-ray energy, 20keV, and sample pressure, 1 GPa, for efficient X-ray induced loss of strontium oxalate crystallinity. We hypothesize that these parameters also represent the optimum parameters for synthesis of CO-derived material from irradiation of strontium oxalate. Additionally, we found that pressurizing the sample generally increased the loss of crystallinity, except when pressurization induced structural changes in the samples. We also hypothesized that X-ray induced loss of crystallinity of strontium oxalate was driven by absorption of an X-ray photon with energy greater than the K-edge of strontium. In chapter three, we corroborated the K-edge dependence of X-ray induced reactions based on experiments on barium and strontium nitrate. We observed that X-rays simultaneously induced local lattice relaxation and decomposition, and through comparison of the X-ray induced effects in barium and strontium nitrate we elucidated the cationic dependence of X-ray photochemistry. These experiments provide significant

insight into some X-ray induced photochemical processes, but they are only the first step towards true optimization of X-ray photochemistry, and much work remains to be done.

The K-edge dependence of X-ray induced reactions that was observed for all studied systems needs to be investigated further. In the experiments described above, we studied X-ray induced reactions at a few energies that varied by a few keV. Based on the few energies that we studied, we got a general picture of the energy dependence. However, future experiments that take advantage of the full energy resolution of monochromatic X-ray systems could provide a fuller picture by investigating many more energies. For example, another study of the energy dependence of X-ray induced decomposition of strontium nitrate could provide additional information by investigating decomposition induced by X-rays of 16.1-16.5 keV rather than 16-22 keV. Additionally, the compounds that we studied were similar in that they were all ionic salts composed of heavy cations and light anions. It is likely that X-ray photochemistry proceeds differently in systems that exhibit different types of atomic/molecular bonding. Future studies on diverse compounds will be needed to investigate such dependencies, but they can be facilitated by following the example set by the experiments described in this thesis. In addition to the k-edge dependence, the pressure dependence of X-ray induced loss of crystallinity that we observed for strontium oxalate must be further verified in other systems.

Based on the results of the pressure dependence of modifications of strontium oxalate, as well as those from previous studies, we concluded that application of pressure dramatically alters X-ray photochemistry. For strontium oxalate, we observed that increasing pressure increases loss of crystallinity except for when pressurization induced structural changes. The results for strontium oxalate were in good agreement with previous studies on TATB^{46, 49}, KClO₃⁴⁷, and KClO₄¹², but further studies on more diverse sets of compounds are required to verify the pressure dependence of X-ray photochemistry. Additionally, future experiments may be able to improve our understanding of the X-ray photochemical

processes at work by investigating X-ray photochemistry in samples that undergo known phase transitions. Such experiments may show that there are some crystalline structures that accommodate X-ray photochemistry more than others. Such knowledge will be critical to refining design of materials intended to mitigate X-ray damage.

New experiments on the pressure dependence of X-ray induced reactions would be greatly simplified by the creation of a new sample chamber that retains the advantages of DAC but is specialized for experiments in X-ray photochemistry at lower pressures. The advantages of using DACs for studying X-ray photochemistry are described in chapter one. To summarize, the DAC provides a sealed, pressurizable, thermally conductive, optically accessible environment in which photochemistry can proceed and be observed. The DAC has two major disadvantages as well, first, the volume of sample produced from X-ray photochemistry experiments are limited by the relatively small culet area and gasket thickness. the limited volume of samples complicates identification of reaction products and cripples the utility of X-ray photochemistry. The second disadvantage is that DAC's are not designed to generate lower pressures that are needed in some X-ray photochemistry experiments. For instance, X-ray induced synthesis of cesium oxide from irradiation of cesium oxalate proceeds differently at 0.4 GPa than at higher pressures.¹⁵ Regularly pressurizing a DAC to a low pressure like 0.4 GPa is a difficult task because our current DACs are designed to achieve much greater pressures. A new type of sample chamber, perhaps as simple as a larger volume DAC, would improve the ability to perform some X-ray photochemistry experiments, and they would enable further studies of the pressure dependence of X-ray photochemistry.

One experiment that we are particularly eager to undertake is the pressure dependence of X-ray included damage of barium and strontium oxalate. As discussed in chapter three, barium and strontium nitrate together are excellent experimental systems for investigating the cationic dependence of parameters that effect X-ray photochemistry, like X-ray energy or the application of pressure. One

particularly interesting aspect of such an experiment would be to investigate the interplay between X-ray induced decomposition and local relaxation of strain. Presumably, these two effects should exhibit different responses to pressurization, and the responses may vary between strontium and barium nitrate as well. Interestingly, since the X-ray induced decomposition of barium and strontium nitrate produces gaseous species, at least when sample pressure is < 0.5 GPa, it is reasonable to suppose that the effect of pressurization on X-ray photochemistry in these systems will be different from that observed for strontium oxalate, which was not observed to produce gaseous species at any sample pressure. Many questions could be answered by performing an experiment on the pressure dependence of barium and strontium oxalate. Besides further investigation of the pressure and energy dependence of X-ray photochemistry, future work is required to investigate other parameters that may affect X-ray photochemistry, like photon flux, temperature, and pressure gradient dependence.

There is preliminary evidence from the studies of barium and strontium nitrate that photon flux or photon flux density may play a role in determining the rate of loss and final loss of crystallinity. We planned and executed experiments to determine the effect of photon flux and flux density on the X-ray induced synthesis of Cesium oxide from irradiation of Cesium oxalate. The experiments were performed from 10/20/2018 to 10/22/2018, and, while the initial results are promising, the data requires additional analysis before findings can be presented confidently. Preliminary results suggest that the rate of loss increases with increasing photon flux density, though the final loss of crystallinity appears to be unaffected by increasing photon flux density. We hope to complete the analysis of this data and submit a paper in the coming months.

Throughout our experiments we have identified two other parameters that may affect X-ray photochemistry: temperature and the pressure gradients. Unfortunately, we are not currently equipped to perform studies on either of these parameters. Controlling temperature in DAC is difficult, particularly

when trying to achieve a stable, precisely measurable temperature at which photochemistry could occur. Many chemical reactions occur differently at high or low temperature, so it is logical to expect that X-ray driven photochemistry may be affected by changing temperature. This affect should be studied, but our group does not currently have the means to do so. Similarly, our group does not currently have to ability to perform experiments to investigate the dependence of X-ray photochemistry on the presence and magnitude of pressure gradients. As mentioned in chapter 1, all the X-ray photochemistry experiments that we have performed thus far involved samples that were loaded in DAC without a pressure transmitting medium (PTM). We do not use a PTM because the presence of another substance, even if that substance is a noble gas like argon, may influence the photochemistry. The lack of PTM implies that there are unavoidable pressure gradients in the samples that we investigated. One way to perform an experiment to investigate the effect of pressure gradients, would be to identify a sample and a PTM that will not react under X-ray irradiation, then to perform studies of that sample with and without the PTM. Unfortunately, the initial identification of a sample and PTM that will not react, is a difficult task that will require several experiments itself. So far, our group has not identified any promising pairs of samples and PTMs. Despite the considerable amount of future work that will be required to achieve the full utility of X-ray photochemistry, the work presented in this thesis is a major first step towards optimization of useful X-ray photochemistry.

The results presented in this thesis, as well as the other experiments mentioned throughout, indicate that X-ray photochemistry can be controlled and optimized. Specifically, we have shown that X-ray induced modifications of strontium oxalate can be controlled by altering the energy of irradiating photons or by pressurizing the sample. We have also shown that X-ray induced decomposition of barium and strontium nitrate exhibits similar response to fluctuations of X-ray energy. Various disciplines can make use of these parameters to regulate or amplify X-ray photochemical processes as necessary, but

they are particularly crucial to the developing field of useful hard X-ray photochemistry. Optimization of useful hard X-ray photochemistry will enable more efficient production of novel materials and may eventually lead to an industrialized process for generating materials that can only be obtained via X-ray irradiation. We look forward to developing X-ray photochemistry further, and to seeing how useful it may become.

References

1. W. Röntgen, *Nature* **53**, 274 (1896).
2. O. Glasser, *W C Rontgen*. (C C Thomas, Springfield, 1958).
3. O. Glasser, *Wilhelm Conrad Roentgen and the Early History of the Roetgen Rays*, 2nd ed. (Jeremy Norman Co, 1992).
4. L. P. Sir Bragg, D.C.; Lipson, H. , *The Development of X-ray Analysis*. (Dover Pubns, 1992).
5. X.-M. Bai, A. F. Voter, R. G. Hoagland, M. Nastasi and B. P. Uberuaga, *Science* **327** (5973), 1631-1634 (2010).
6. H. Matzke, *Nuclear Instruments and Methods in Physics Research Section B: Beam Interactions with Materials and Atoms* **65** (1-4), 30-39 (1992).
7. *Radiation Effects in Solids*. (Springer Science, 2007).
8. R. F. Martin and L. E. Feinendegen, *International journal of radiation biology* **92** (11), 617-632 (2016).
9. M.-C. Biston, A. Joubert, J.-F. Adam, H. Elleaume, S. Bohic, A.-M. Charvet, F. Estève, N. Foray and J. Balosso, *Cancer research* **64** (7), 2317-2323 (2004).
10. B. A. McGuire, A. M. Burkhardt, S. Kalenskii, C. N. Shingledecker, A. J. Remijan, E. Herbst and M. C. McCarthy, *Science* **359** (6372), 202-205 (2018).
11. M. Pravica, D. Sneed, Q. Smith and L. Bai, *Chemical Physics Letters* **590**, 74-76 (2013).
12. M. Pravica, Y. Wang, D. Sneed, S. Reiser and M. White, *Chemical Physics Letters* **660**, 37-42 (2016).
13. M. Pravica, D. Sneed, M. White and Y. Wang, *Review of Scientific Instruments* **85** (8), 086110 (2014).
14. F. Lu, Z. Dong, J. Zhang, T. White, R. Ewing and J. Lian, *Tailoring the Radiation Tolerance of Vanadate-Phosphate Fluorapatites by Chemical Composition Control*. (2013).
15. E. Evlyukhin, E. Kim, D. Goldberger, P. Cifligu, S. Schyck, P. F. Weck and M. Pravica, *Physical Chemistry Chemical Physics* (2018).
16. M. Pravica, M. White and Y. Wang, *AIP Conference Proceedings* **1793** (1), 060030 (2017).
17. M. Maosheng, B. Jorge, P. Michael, S. Daniel and P. Changyong, *Japanese Journal of Applied Physics* **56** (5S3), 05FA10 (2017).
18. A. Smale, in *Nasa's Imagine the Universe*, edited by M. J.D. (Nasa, 2013).
19. F. R. Elder, A. M. Gurewitsch, R. V. Langmuir and H. C. Pollock, *Physical Review* **71** (11), 829-830 (1947).
20. (The European Synchrotron Facility).
21. M. H. J. Koch and J. Bordas, *Nuclear Instruments and Methods in Physics Research* **208** (1), 461-469 (1983).
22. in *About the APS*, Vol. 2018.
23. H. Winick, G. Brown, K. Halbach and J. Harris, *Physics Today* **34** (5), 50-63 (1981).
24. C. Park and D. Popov, (2018), Vol. 2018.
25. P. Eisenberger and P. Platzman, *Physical Review A* **2** (2), 415 (1970).
26. A. Guinier, *X-ray Diffraction: In Crystals, Imperfect Crystals, and Amorphous Bodies*. (Dover Publications, 1994).
27. J. T. Bushberg and J. M. Boone, *The essential physics of medical imaging*. (Lippincott Williams & Wilkins, 2011).
28. C. G. Barkla, *The London, Edinburgh, and Dublin Philosophical Magazine and Journal of Science* **22** (129), 396-412 (1911).

29. J. Matthew and Y. Komninos, *Surface Science* **53** (1), 716-725 (1975).
30. K. Gokhberg, P. Kolorenč, A. I. Kuleff and L. S. Cederbaum, *Nature* **505** (7485), 661 (2014).
31. J. Zobeley, R. Santra and L. S. Cederbaum, *The Journal of Chemical Physics* **115** (11), 5076-5088 (2001).
32. W. H. Bragg and L. Bragg, *Proceedings of the Royal Society of London. Series A* **88** (605), 428-438 (1913).
33. R. J. Haüy, *Traité de Minéralogie*. (Paris France, 1801).
34. W. H. Miller, *A Treatise on Crystallography*. (J. & J.J. Deighton, Cambridge, 1839).
35. P. Debye, *Annalen der Physik* **351** (6), 809-823 (1915).
36. C. Prescher and V. B. Prakapenka, *High Pressure Research* **35** (3), 223-230 (2015).
37. P. R. G. D. J. Graves, *Practical Raman Spectroscopy*. (Springer-Verlag Berlin Heidelberg, 1989).
38. A. Dewaele, P. Loubeyre, F. Occelli, O. Marie and M. Mezouar, *Nature communications* **9** (2018).
39. F. S. Isaac and D. Ranga, *Journal of Physics: Condensed Matter* **30** (25), 254003 (2018).
40. H. Mao, J.-A. Xu and P. Bell, *Journal of Geophysical Research: Solid Earth* **91** (B5), 4673-4676 (1986).
41. A. Dewaele, M. Torrent, P. Loubeyre and M. Mezouar, *Physical Review B* **78** (10), 104102 (2008).
42. S. Klotz, J. Chervin, P. Munsch and G. Le Marchand, *Journal of Physics D: Applied Physics* **42** (7), 075413 (2009).
43. M. Pravica, D. Sneed, Q. Smith, B. Billingham, T. May, M. White and K. Dziubek, *Cogent Physics* **3** (1) (2016).
44. M. Pravica, E. Evlyukhin, P. Cifligu, B. Harris, J. J. Koh, N. Chen and Y. Wang, *Chemical Physics Letters* **686**, 183-188 (2017).
45. M. Pravica, L. Bai, D. Sneed and C. Park, *The Journal of Physical Chemistry A* **117** (11), 2302-2306 (2013).
46. H. Giefers and M. Pravica, *The Journal of Physical Chemistry A* **112** (15), 3352-3359 (2008).
47. M. Pravica, L. Bai and N. Bhattacharya, *Journal of Applied Crystallography* **45** (1), 48-52 (2012).
48. D. Goldberger, E. Evlyukhin, P. Cifligu, Y. Wang and M. Pravica, *The Journal of Physical Chemistry A* **121** (38), 7108-7113 (2017).
49. H. Giefers, M. Pravica, H.-P. Liermann and W. Yang, *Chemical Physics Letters* **429** (1-3), 304-309 (2006).
50. E. D. Bacce, A. M. Pires, M. R. Davalos and M. Jafellici Jr, *International Journal of Inorganic Materials* **3** (6), 443-452 (2001).
51. D. J. Price, A. K. Powell and P. T. Wood, *Polyhedron* **18** (19), 2499-2503 (1999).
52. Y. W. Yin, *Journal of the American Chemical Society* **126** (45), 14996-14996 (2004).
53. M. Avrami, *The Journal of Chemical Physics* **8** (2), 212-224 (1940).
54. M. Avrami, *The Journal of Chemical Physics* **7** (12), 1103-1112 (1939).
55. D. Chelazzi, M. Ceppatelli, M. Santoro, R. Bini and V. Schettino, *The Journal of Physical Chemistry B* **109** (46), 21658-21663 (2005).
56. E. Evlyukhin, L. Museur, M. Traore, C. Perruchot, A. Zerr and A. Kanaev, in *Sci Rep* (2015), Vol. 5, pp. 18244.
57. C. S. Yoo and M. Nicol, *The Journal of Physical Chemistry* **90** (25), 6732-6736 (1986).
58. C. Rischel, A. Rousse, I. Uschmann, P.-A. Albouy, J.-P. Geindre, P. Audebert, J.-C. Gauthier, E. Fröster, J.-L. Martin and A. Antonetti, *Nature* **390** (6659), 490 (1997).
59. Y. Matsui, K. Sakai, M. Murakami, Y. Shiro, S.-i. Adachi, H. Okumura and T. Kouyama, *Journal of molecular biology* **324** (3), 469-481 (2002).
60. A. Jena and M. C. Chaturvedi, *Phase transformation in materials*. (Prentice Hall, 1992).

61. C. Lehmann, A. Picón, C. Bostedt, A. Rudenko, A. Marinelli, D. Moonshiram, T. Osipov, D. Rolles, N. Berrah and C. Bomme, *Physical Review A* **94** (1), 013426 (2016).
62. M. Hoener, L. Fang, O. Kornilov, O. Gessner, S. T. Pratt, M. Gühr, E. P. Kanter, C. Blaga, C. Bostedt and J. D. Bozek, *Physical review letters* **104** (25), 253002 (2010).
63. A. Picón, C. Lehmann, C. Bostedt, A. Rudenko, A. Marinelli, T. Osipov, D. Rolles, N. Berrah, C. Bomme and M. Bucher, *Nature communications* **7**, 11652 (2016).
64. J. Cunningham and H. Heal, *Transactions of the Faraday Society* **54**, 1355-1369 (1958).
65. A. Rudenko, L. Inhester, K. Hanasaki, X. Li, S. J. Robotjazi, B. Erk, R. Boll, K. Toyota, Y. Hao, O. Vendrell, C. Bomme, E. Savelyev, B. Rudek, L. Foucar, S. H. Southworth, C. S. Lehmann, B. Kraessig, T. Marchenko, M. Simon, K. Ueda, K. R. Ferguson, M. Bucher, T. Gorkhover, S. Carron, R. Alonso-Mori, J. E. Koglin, J. Correa, G. J. Williams, S. Boutet, L. Young, C. Bostedt, S. K. Son, R. Santra and D. Rolles, *Nature* **546**, 129 (2017).
66. D. Goldberger, C. Park, E. Evlyukhin, P. Cifligu and M. Pravica, *The Journal of Physical Chemistry A* (2018).
67. H. Nowotny and G. Heger, *Acta Crystallographica Section C: Crystal Structure Communications* **39** (8), 952-956 (1983).
68. A. Thompson and D. Vaughan, Lawrence Berkeley National Laboratory (2001).
69. W. H. McMaster, N. K. Del Grande, J. Mallett and J. Hubbell, 1969.
70. V. Stumpf, K. Gokhberg and L. S. Cederbaum, *Nature chemistry* **8** (3), 237 (2016).
71. K. Momma and F. Izumi, *Journal of Applied Crystallography* **44** (6), 1272-1276 (2011).
72. R. Hrubyak, S. Sinogeikin, E. Rod and G. Shen, *Review of Scientific Instruments* **86** (7), 072202 (2015).
73. J. Zhao, G. Hearne, M. Maaza, M. K. Nieuwoudt and J. D. Comins, *Review of Scientific Instruments* **71** (12), 4509-4511 (2000).
74. P. G. Zverev, J. T. Murray, R. C. Powell, R. J. Reeves and T. T. Basiev, *Optics Communications* **97** (1), 59-64 (1993).
75. D. d. Waal, K. J. Range, M. Königstein and W. Kiefer, *Journal of Raman Spectroscopy* **29** (2), 109-113 (1998).
76. R. Hill, P. Esherick and A. Owyong, *Journal of Molecular Spectroscopy* **100** (1), 119-133 (1983).
77. C. Park, D. Popov, D. Ikuta, C. Lin, C. Kenney-Benson, E. Rod, A. Bommannavar and G. Shen, *Review of Scientific Instruments* **86** (7), 072205 (2015).
78. R. A. Young, *The rietveld method*. (International union of crystallography, 1993).

Curriculum Vitae

David L. Goldberger
Email: David.Goldberger@Colorado.edu

Education

University of Colorado at Boulder (CU) — Boulder, CO 2011 - 2015
B.A. Physics, B.F.A Theatrical Performance (Acting) Cumulative GPA 3.842, Summa Cum Laude

University of Nevada at Las Vegas (UNLV) — Las Vegas, NV 2017 - Present
M.S. Physics Current GPA 4.0

Research Interest

Useful Hard X-ray Photochemistry particularly X-ray induced decomposition reactions and synthesis of novel materials. AMO physics, particularly atom trapping and BECs. Quantum computing, and physics education.

Scientific Employment

Graduate Research Assistant, UNLV 2017 - Present

Research in Hard X-ray Photochemistry with Dr. M. Pravica

- Designed and execute X-ray induced decomposition and synthesis experiments at the Advanced Photon Source (APS) at Argonne National Lab - to date: 36 shifts (288 hours) of beam-time at APS
- Prepare samples in Diamond Anvil Cells (DACs) for study at high pressure
- Analyze samples with XRD and associated software (Dioptas, GSAS, etc.)
- Analyze samples with Raman Spectroscopy and associated software (LabSpec, Winspec, etc.)
- Compile and analyze data independently using Origin and other similar programs

Undergraduate Research Assistant, JILA/CU 2013 - 2015

Research in Bose-Einstein Condensates with Drs. E. Cornell and D. Jin

- Undergraduate Thesis Project "Improving Imaging Resolution For In-Situ Measurements of Bose-Einstein Condensates", Designed complex multi-lens imaging system
- Design and fabricate circuits and mechanical components (temperature interlock, laser frequency servo, laser cooling block, custom rack system etc.)
- Analyze BEC data and compared to self-written theoretical model.

Publications

Goldberger D., Park C., Evlyukhin E., Cifligu P., Pravica M., Cationic Dependence of X-ray Induced Damage of Strontium and Barium Nitrate, Journal of Physical Chemistry A 2018

Evlyukhin E., Kim E., Cifligu P., **Goldberger D.**, Schyck S., Harris B., Torres S., Rossman G., Pravica M., Synthesis of a Novel Strontium-based Wide-Bandgap Semiconductor Via X-ray Photochemistry at Extreme Conditions, Journal of Materials Chemistry C 2018 (in review)

Evlyukhin E., Kim E. **Goldberger D.**, Cifligu P., Schyck S., Weck P., Pravica M., HighPressure-Assisted X-ray-Induced Damage as a New Route for Chemical and Structural Synthesis, Journal of Physical Chemistry and Chemical Physics 2018

Goldberger D., Evlyukhin E., Cifligu P., Wang Y., Pravica M., Measurement of the Energy and High-Pressure Dependence of X-ray-Induced Decomposition of Crystalline Strontium Oxalate, Journal of Physical Chemistry A 2017

Makotyn P., Klauss CE., **Goldberger DL.**, Cornell EA., Jin DS., Universal Dynamics of a Degenerate Bose Gas, Nature Physics 2014

Teaching Experience

UNLV 151, 152 Lab (Fall 2017, Spring and fall 2018)
Introductory and intermediate Physics labs for pre-med and other general education students

UNLV 181, 182 Lab (Fall 2017, Fall 2018)
Intermediate Physics labs for engineers and physicists

Instructor with Play-Well TEKnologies (2016 - 2017)
Taught fundamentals of engineering to K-8th graders through play with Legos

Private Tutoring (2014 - present)
High-school and college physics, calculus, trigonometry, etc.